Chapter 3

Some properties of the local clouds

3.1 Introduction

Although the primary objective of this thesis is a detailed kinematical study of the local dark clouds (to be taken up in Chapters 4 and 5), in this chapter we present some statistical distributions of the line strengths and linewidths obtained by us. Since we have observed a large number of clouds distributed over all longitudes, this population is ideally suited for a study of the *average physical conditions prevailing in these clouds.* Most of the clouds were observed at only one position, but as the observed positions were close to the centres of these clouds the spectra obtained are likely to be representative of the whole clouds. While a detailed analysis of the distributions to be presented is outside the scope of this thesis, we would like to point out what we consider to be some interesting trends leading to some tentative suggestions.

3.2 The distribution of kinetic temperatures

The kinetic temperatures of molecular clouds are usually determined from the peak line strengths of ^{12}CO. This makes sense because the ^{12}CO line is invariably optically thick. However, a disadvantage of this method is that precisely for this reason one will be predominantly sampling the outer regions of the clouds and hence one has to make some assumptions about the temperature distribution inside the cloud.

Keeping in mind that the usual Rayleigh-Jeans approximation ($h\nu << kT$) is not valid at millimeter wavelengths for the typical kinetic temperatures that obtain

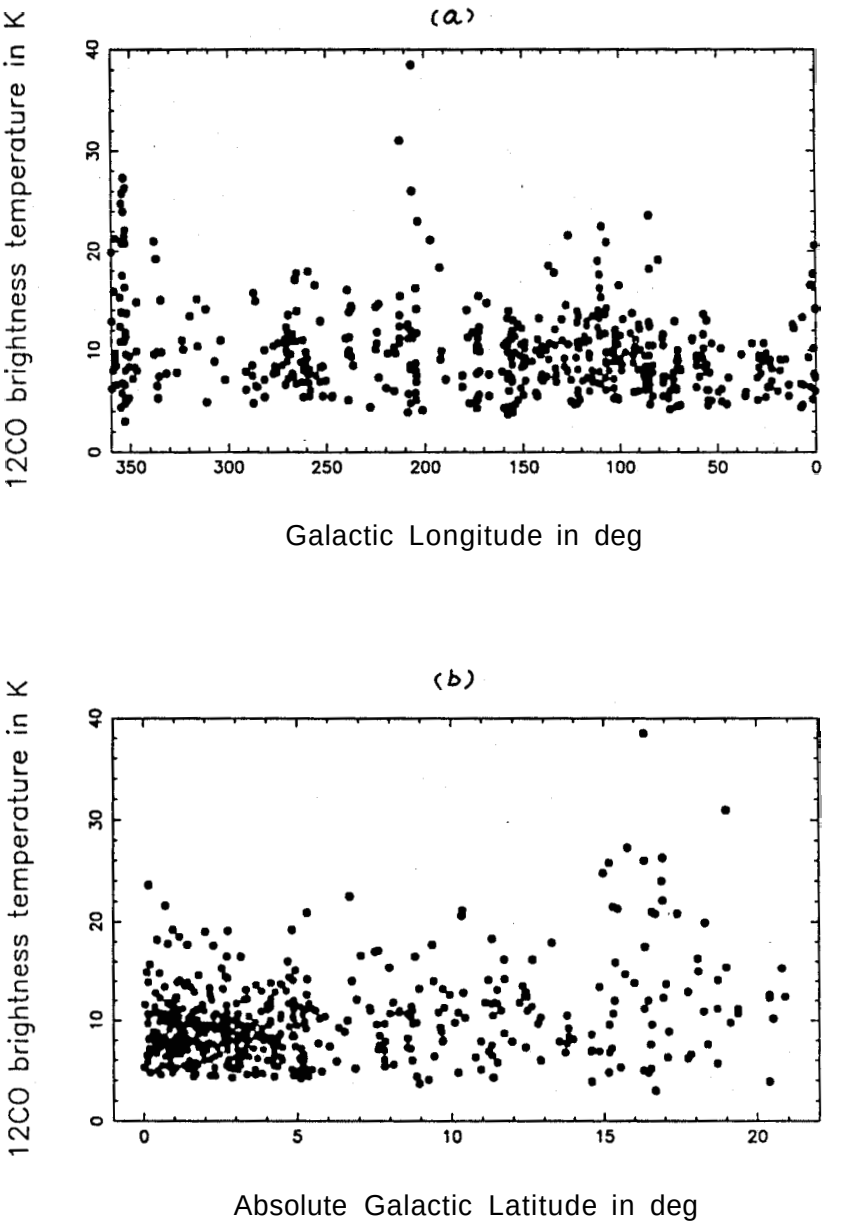

Fig.3.1 : Longitude and latitude distributions of the ^{12}CO source brightness temperatures of the local clouds are shown in (a) and (b) respectively.

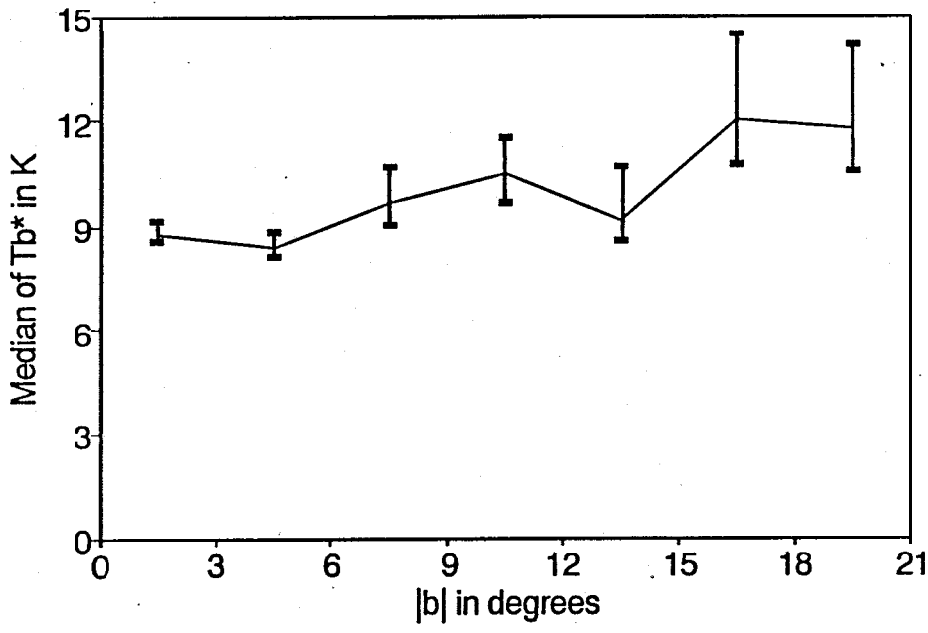

Fig.3.1.c : The latitude distribution of the median of the ^{12}CO brightness temperatures of the local dark clouds is displayed. The clouds have been binned in 3° latitude segments. The errors on the median are $\frac{\sigma_T}{\sqrt{N}}$ where σ_T is the dispersion in the temperature distribution in the bin and N is the number of clouds in that bin. To take into account the asymmetry in the distribution, two rms errors have been computed, one on either side of the median value. The median of the brightness temperature shows a marginal increase with latitude.

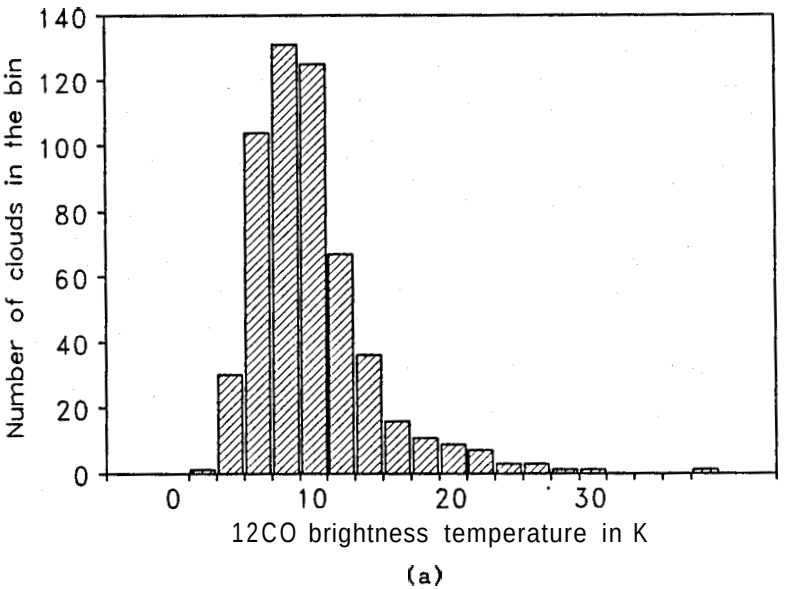

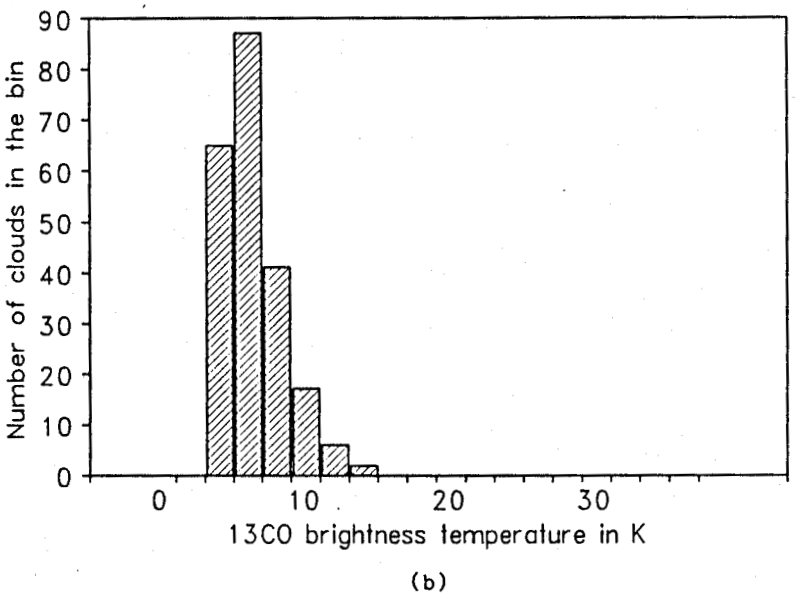

Fig.3.2 : Histograms of the ^{12}CO and ^{13}CO source brightness temperatures are shown in (a) and (b) respectively.

in these clouds, and taking into account the 2.7 K background, the peak ^{12}CO line strength can be related to the kinetic temperature as given below (Dickman, 1978):

$$T_{kin} = \frac{5.532}{ln\left(1 + \frac{5.532}{\left(\frac{T_A^*}{\eta_{fss}} + 0.8182\right)}\right)} = T_{ex}\left(^{12}CO\right) \qquad (3.1)$$

Here η_{fss} is the forward spillover and scattering efficiency. We estimate this to be 0.57 and 0.63 at the ^{12}CO and ^{13}CO frequencies, respectively, by comparing the measured antenna temperatures on the calibration sources with the source brightness temperatures reported in the literature.

The longitude and latitude distributions of the kinetic temperatures, derived from the ^{12}CO line strengths, are shown in figures 3.1.a and 3.1.b, respectively. Figure 3.1.c shows the plot of the median temperatures vs latitude along with estimated rms errors on them. The median values have been computed by binning the clouds into 3° latitude segments. The rms error values are $\frac{\sigma_T}{\sqrt{N}}$ where σ_T is the rms dispersion of the temperature distribution of the clouds in a latitude bin and N is the number of clouds in that bin. Since the distribution is asymmetric we have computed two rms error values, one on either side of the median value. As will be seen, the temperature appears to increase with the latitude but not in a very pronounced manner. The tentative interpretation is that the clouds at higher latitudes possibly have higher heating rate or lower cooling rate or both. The heating rate can be more if the general interstellar radiation field at high Z is more than that at the plane. The cooling is also possibly slower because the dominant cooling process in small molecular clouds viz. "cooling due to lines" depends on the density as well as the temperature of the cloud as $7 \times 10^{-30}\ T^{2.2}\ n(H_2)$ (Goldsmith and Langer, 1978). The clouds at high latitudes have lesser number density which leads to slightly higher equilibrium kinetic temperature.

Another noticeable feature is that while most of the clouds have kinetic temperatures between 5 K and 15 K, typical of the small dark clouds, some clouds in the longitude ranges $85° - 140°, 190° - 215°$ and $345° - 5°$ are somewhat warmer. This trend is also to be found in the composite CO survey map of Dame et al. (1987) in the longitude range $85° - 140°$. Concerning the other two directions, it will be recalled that the Orion and Sco-Cen OB associations are to be found there. Hence the higher kinetic temperatures of the clouds in these directions should presumably be understood in terms of local heating due to the OB associations. The histograms of the ^{12}CO and ^{13}CO brightness temperatures are shown in figure 3.2.

3.3 Latitude dependence of the linewidths

In Figure 3.3.a and 3.3.b we have shown the ^{12}CO linewidths (W12) plotted against the longitudes and latitudes of the clouds. While the longitude distribution does

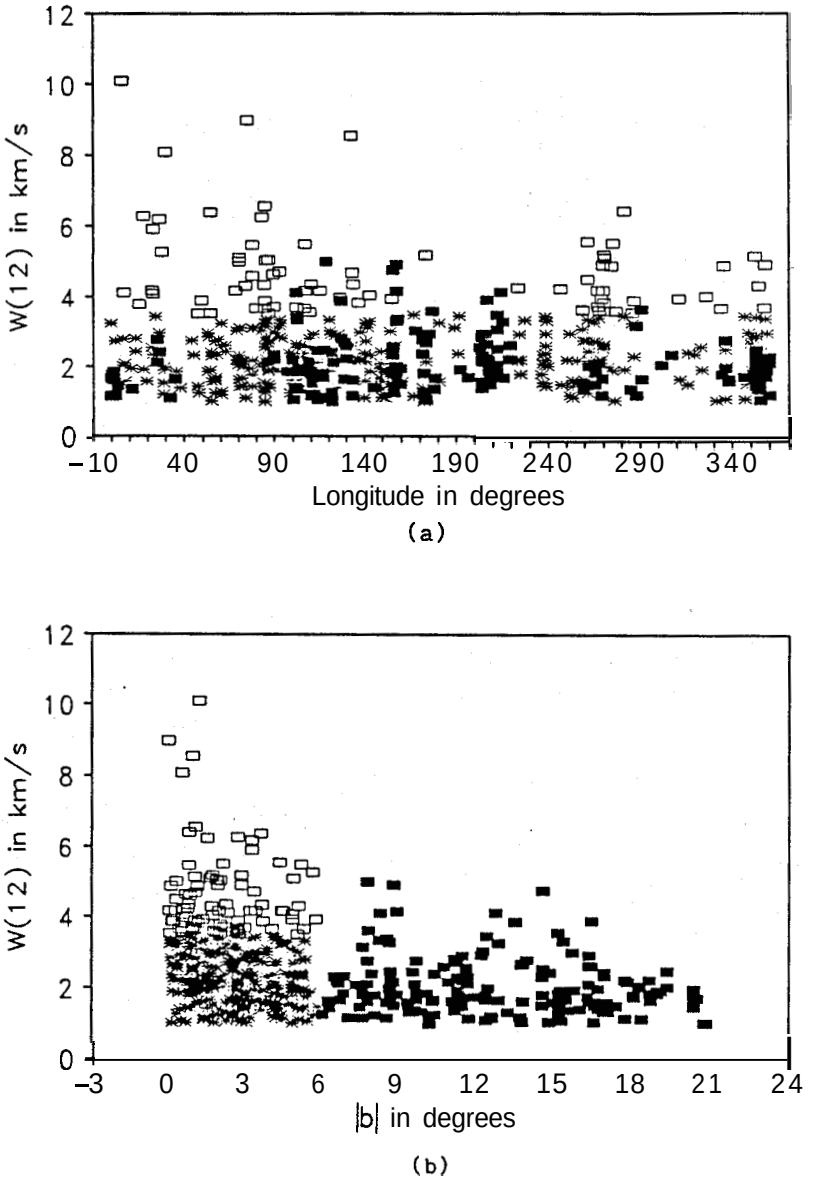

Fig.3.3 : ^{12}CO line widths versus longitudes is shown in (a). Their latitude distribution is shown in (b). The clouds, with $|b| < 6'$ and $W(12) < 3.5$ km/s are shown by "$\star$". Open squares represent clouds with $|b| < 6'$ and $W(12) > 3.5$ km/s. Filled squares denote clouds with $|b| > 6°$.

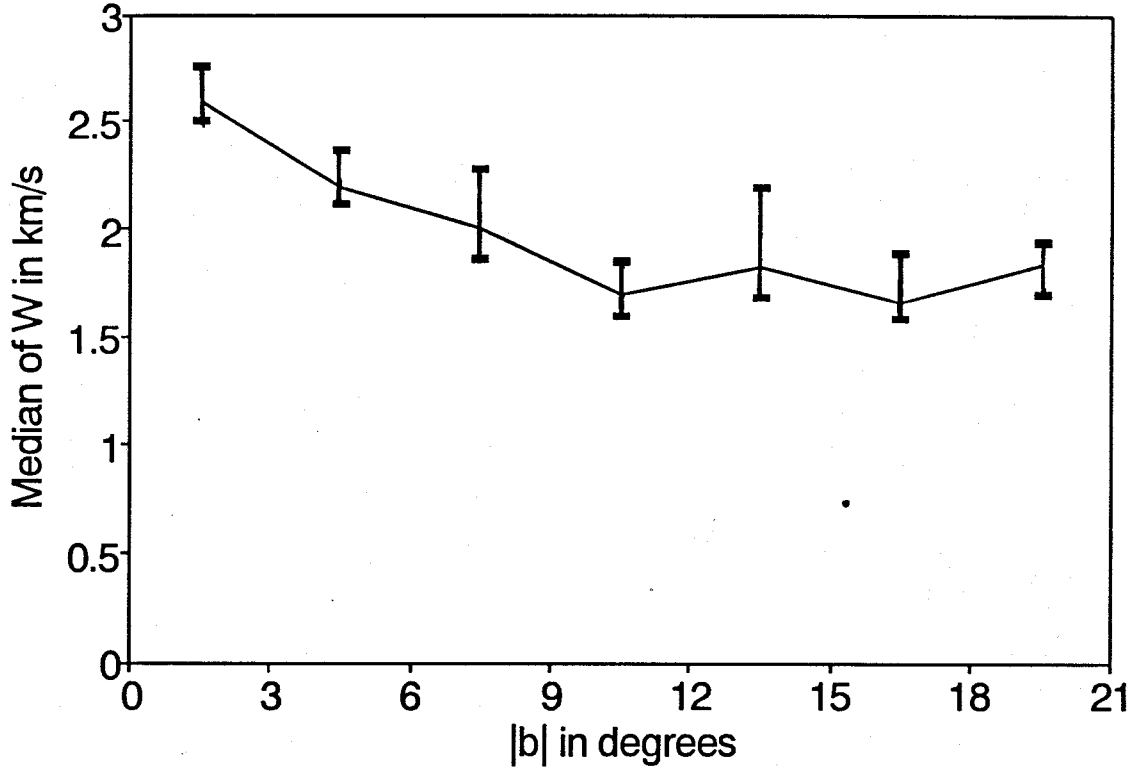

Fig.3.3.c : Figure shows the latitude distribution of the median of the ^{12}CO linewidths. The data has been binned and the error values have been calculated in the same way as were done for the brightness temperatures. Clearly, the median of the ^{12}CO linewidths increases with latitude.

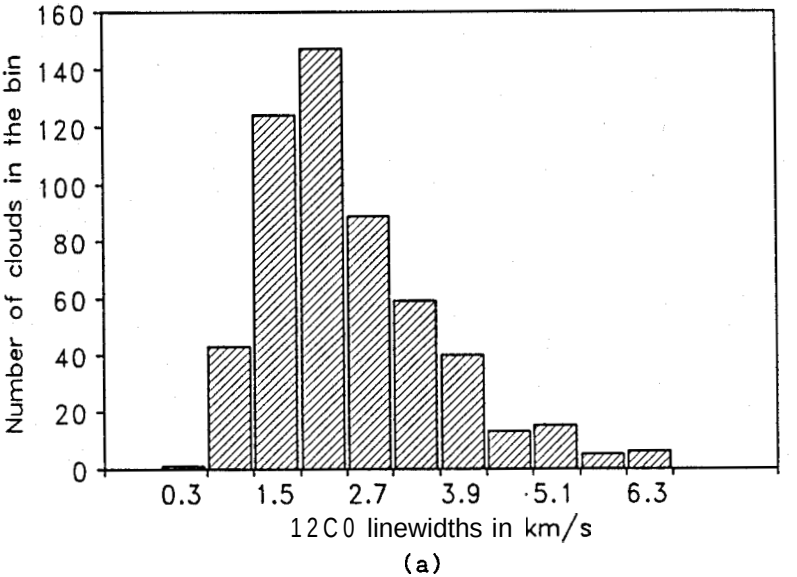

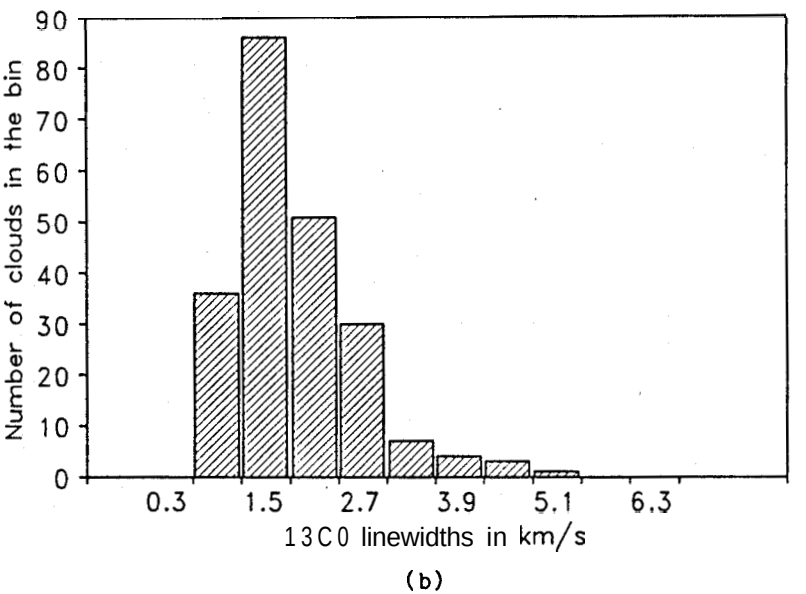

Fig.3.4 : Histograms of ^{12}CO and ^{13}CO line widths are shown in (a) and (b) respectively.

not show any particular trend, a decrease in width with increasing latitude is seen in the latitude distribution. In order to show that this is not an artefact caused by any specific set of clouds confined to a certain range of longitude but is a general feature we have plotted the population of clouds using three different symbols: those with $|b| < 6°$, $(W12) < 3.5$ kms^{-1} are represented by $\star$s, those with $|b| < 6°$, but $(W12) > 3.5$ kms^{-1} are denoted by open squares, and those with $|b| > 6°$ by filled squares. As will be noticed, it is the clouds represented by the open squares and the filled squares that accentuate any decreasing trend in linewidths with increase in latitude. But an inspection of figure 3.3.a will show that these clouds are distributed over all the longitudes and the trend seen in figure 3.3.b must be regarded as real. One might also wonder if the trend is not because of the lesser number of clouds at higher latitudes and hence lesser chance of clouds with larger width being seen - a matter of statistical fluctuation. Figure 3.3.c shows the plot of the median linewidths vs latitude along with estimated rms errors on them. The median and the error values have been computed in the same way as was done in the case of temperature. Clearly, the median linewidths decrease with latitude.

Such a latitude dependence may arise in one of two ways. The observed linewidths are most likely due to turbulence within the clouds.If the clouds are in *virial equilibrium* (Bally, 1989), then the linewidths will be related to the masses of the clouds. And if the clouds at higher latitudes are interpreted as being at greater z-distances from the galactic plane, then the observed trend may be understood in terms of a tendency towards equipartitioning of the kinetic energies of the clouds. Under these circumstances, the clouds with smaller masses will have higher velocities and therefore can be expected to be found at greater distances from the galactic plane (Scoville et al., 1987).

There may also be an alternative explanation. The turbulence responsible for the line-widths could also be caused by galactic spiral density waves (Thomasson et al., 1989). If this is indeed the case then it is conceivable that the effect of the spiral density wave is less pronounced in clouds at a greater distance from the galactic plane. The two scenarios we have mentioned are admittedly very simplistic, but in our opinion the decreasing trend seen in figure 3.3.c is worth investigating in a more systematic fashion. To conclude this section we present in figure 3.4 the histograms of the ^{12}CO and ^{13}CO linewidths.

3.4 The distribution of ^{13}CO column densities

Assuming that ^{13}CO is optically thin, and that both ^{12}CO and ^{13}CO have the same excitation temperatures, one can obtain the ^{13}CO optical depth using the standard equations of radiative transfer. The expression for the optical depth is given by (Dickman, 1978):

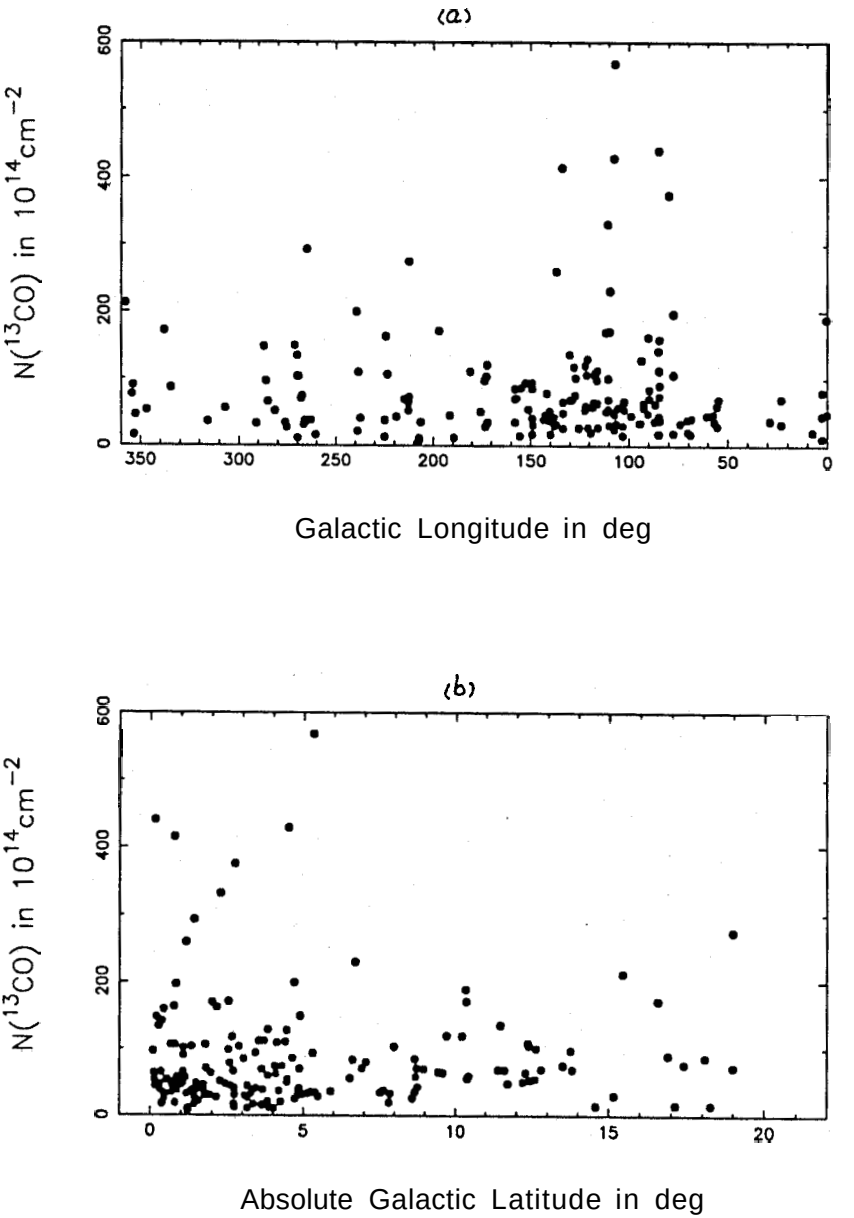

Fig.3.5 : Distributions of ^{13}CO column densities in longitude and latitude are shown in (a) and (b) respectively.

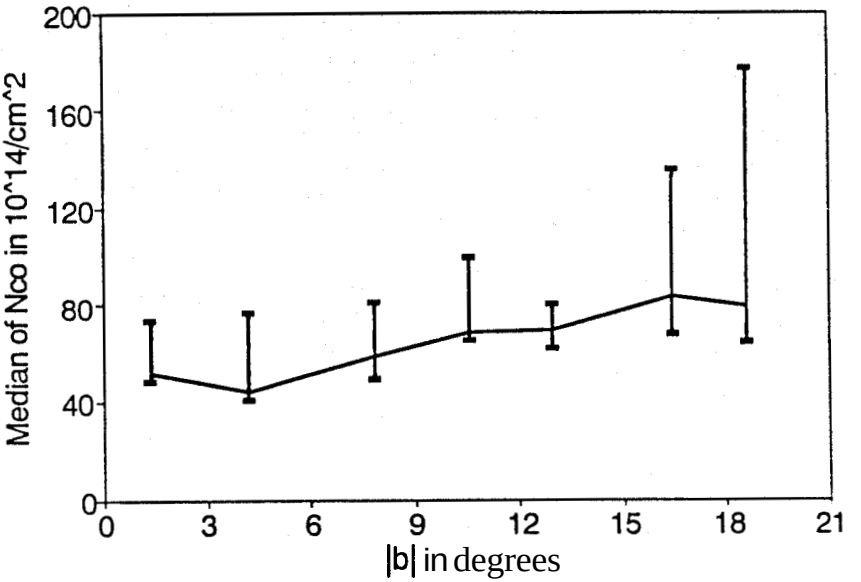

Fig.3.5.c : Distribution of the median of ^{13}CO column densities us latitude. Following the same procedure as was used with temperatures and linewidths, the data has been binned and the error values have been calculated. Possibly, the median of the ^{13}CO column densities increases with latitude. But, it should be noted that the number of clouds in the higher latitude bins are not many, and the effects of small number statistics can be significant.

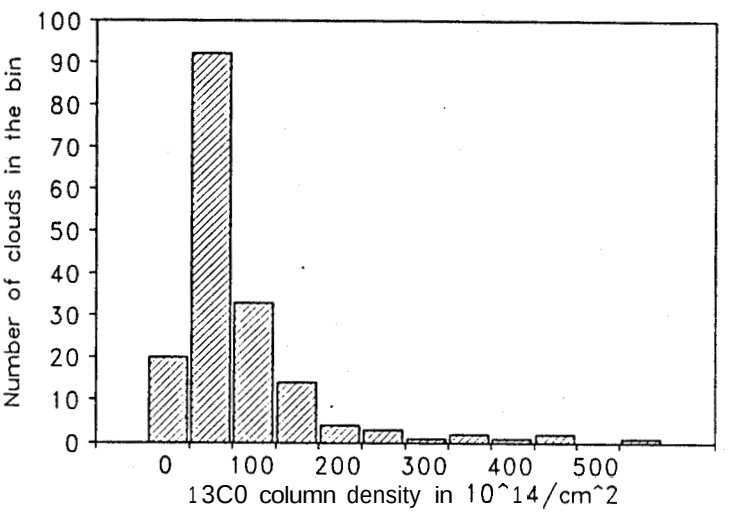

Fig.3.6 : Histogram of ^{13}CO column densities.

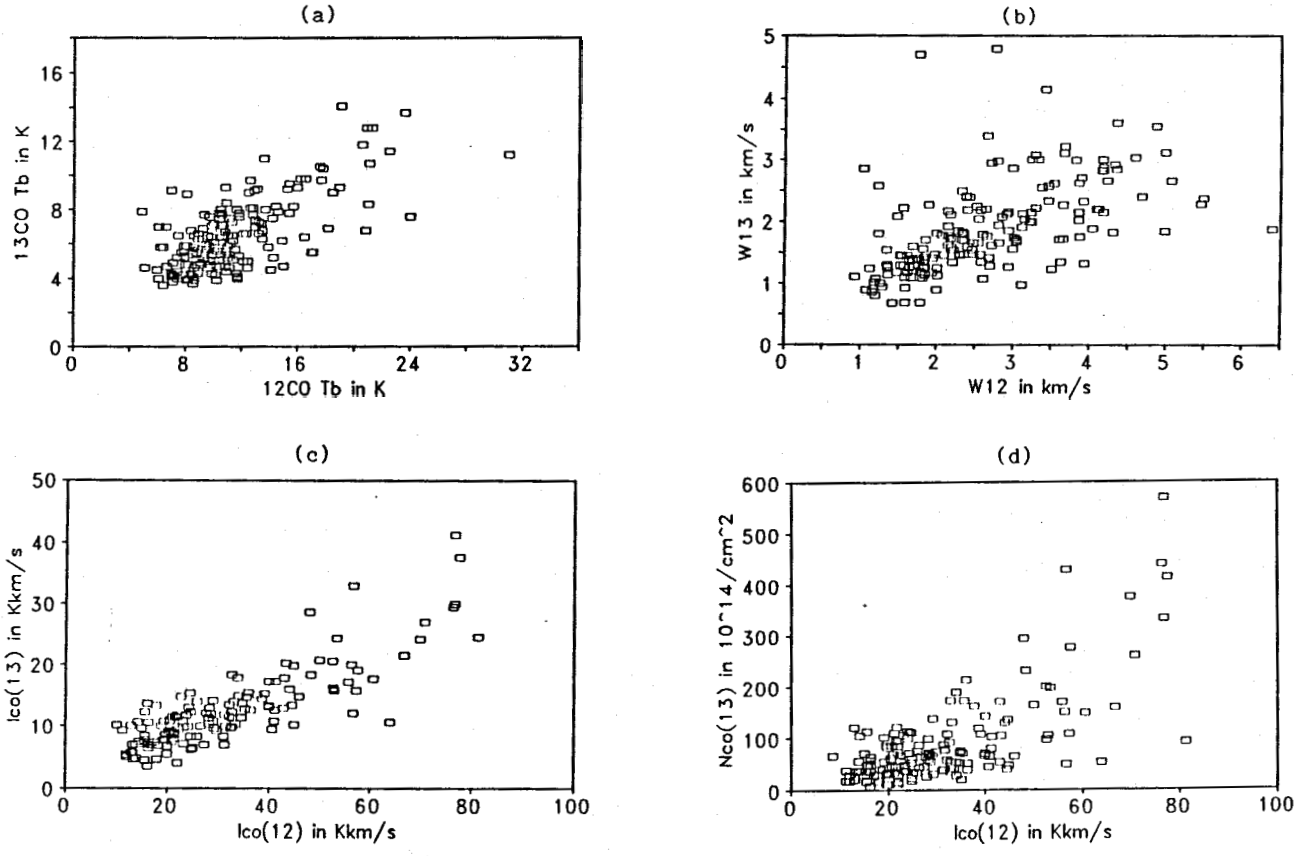

Fig.3.7 : Correlation between ^{12}CO and ^{13}CO source brightness temperatures is shown in (a) and that between the respective line widths is shown in (b). Figure (c) shows the correlation between the ^{12}CO and ^{13}CO integrated line intensities. The ^{13}CO column density *versus* ^{12}CO integrated line intensity plot is shown in (d).

$$\tau_{13} = -ln\left[1 - \frac{T_{13}}{5.289\left\{\left[e^{\frac{5.289}{T_{ex}}} - 1\right]^{-1} - 0.1642\right\}}\right] \tag{3.2}$$

The ^{13}CO column density is given by

$$N_{^{13}CO} = 2.42 \times 10^{14} \times \frac{T_{ex}\tau_{13}W(13)}{(1 - e^{-5.289/T_{ex}})} \tag{3.3}$$

where W(13) is the FWHM of ^{13}CO line, and T_{ex} is the excitation temperature obtained from the peak ^{12}CO line strength.

The longitude and the latitude distributions of the ^{13}CO column densities derived using the above relations are shown in figure 3.5. The median plot of the ^{13}CO column densities is plotted in figure 3.5.c. Possibly there is an increasing trend with latitude. However, at higher latitudes the number of measured points are few and hence the effects of small number statistics can not be ignored. Nevertheless, the apparent trend does warrant a systematic investigation. A few clouds with latitudes less than 6° and column densities in excess of $\sim 300 \times 10^{14}$ cm^{-2} are likely to belong to the tail end of the distribution, there being a large population of clouds in the plane. But, we wish to note that they all lie in the longitude range 85° – 140° where, as will be argued in the next chapter, the clouds are predominantly coming towards us unlike those in the other longitudes which are receding from us. A histogram of ^{13}CO column densities is shown in figure 3.6.

3.5 Correlations among the various parameters

In figure 3.7.a we have plotted the ^{13}CO brightness temperatures against the corresponding ^{12}CO brightness temperatures. While the latter are likely to be equal to the kinetic temperatures, the brightness temperature of the optically thin ^{13}CO lines will be a product of the kinetic temperatures and the ^{13}CO optical depths, and this is what figure 3.7.a indicates. The scatter in the diagram presumably results from the variation of optical depth from cloud to cloud, but it should be noted that the scatter is fairly small.

The correlation between the ^{12}CO and ^{13}CO linewidths is shown in figure 3.7.b. The scatter is larger in this plot, and most of the points lie below the expected line of 45°, slope. We wish to mention in passing that one may be seeing the effects of optical depth variations within the cloud, such as due to mass segregation. If the more massive clumps in the molecular clouds sink towards their centres (perhaps due to equipartition?), then one can in principle understand the trend seen in figure 3.7.b. In this scenario the ^{12}CO linewidths will be dominated by the less massive clumps in the outer regions, while the ^{13}CO linewidths sample even the more massive clumps near the centre.

Figure 3.7.c shows the correlations between the ^{12}CO and ^{13}CO integrated line intensities (which are the product of the respective brightness temperatures and the linewidths). The most noteworthy feature of this figure is that there is a much tighter correlation in the integrated line intensities compared to what is seen in figure 3.7.a and 3.7.b.

Figure 3.7.d shows the ^{13}CO *column* density *vs* ^{12}CO integrated line intensities. The ^{12}CO integrated line intensities have often been used in the literature to estimate the masses of the clouds. This would require that the ^{12}CO integrated line intensity and the ^{13}CO column density to be linearly related. But our figure shows that this is not the case – there is a considerable scatter. However, there is clearly an upper envelope to this distribution. The various correlation coefficients obtained from the distributions presented so far are given in Table 3.1.

Table 3.1 : Correlation coefficients

Parameter	Slope	Dispersion
$T_b(12)$ vs $T_b(13)$	0.60	1.1 K
W(12) vs W(13)	0.65	0.6 kms^{-1}
$I_{CO}(12)$ vs $I_{CO}(13)$	0.40	2.2 K kms^{-1}

References

Bally, J. 1989, in Low Mass Star Formation and Pre-Main Sequence Objects, ESO Conference and Workshop Proceedings No.33, ed.B.Reipurth.

Dame, T.M, Ungrechts, H., Cohen, R.S., de Geus, E.J., Grenier, I.A., May, J., Murphy, D.C., Nyman, L.A., Thaddeus, P. 1987, *Astrophys.J.*, 322, 706.

Dickman, R.L., 1978, *Astrophys.J.Suppl.*, 37, 407.

Goldsmith, P.F., Langer, W.D., 1978, *Astrophys.J.*, 222, 881.

Scoville, N.Z., Yun, M.S., Clemens, D.P., Sanders, D.B., Waller, W.H. 1987, *Astrophys.J.Suppl.*, 63, 821.

Thomasson, M., Donner, K.J., Elmegreen, B.G. 1991, *Astr.Astrophys.*, 250, 316.

Chapter 4

Kinematical Analysis and Simulations

4.1 Introduction

In the previous chapter we discussed the average physical properties of the local dark clouds and their interpretation. In this chapter we analyse the radial velocities of the local dark clouds in various longitudes to understand their kinematical behaviour.

The basic aims of this chapter are the following:

1. To investigate whether the local system of dark clouds are in a state of expansion about a common center.
2. To estimate the magnitude of the peculiar velocities of the clouds.
3. To test the above conclusions from an analysis of a subset of clouds with known distances.
4. To derive the spatial distribution of the local dark clouds.

The distribution of the clouds on the sky is shown in Fig.4.1.a, and Fig.4.1.b is their longitude-velocity plot. The "double sinusoidal" behaviour seen in Figure 4.1.b clearly shows that the contribution of galactic differential rotation is important. We estimate these contributions using the equation

$$V_{rot}(l) = Ad\sin(2l) \tag{4.1}$$

with a value of 14.5 $kms^{-1}kpc^{-1}$ for Oort's constant **A.** Here d is the distance and 1 is the longitude of the cloud. We have omitted a factor $\cos^2 b$ in this

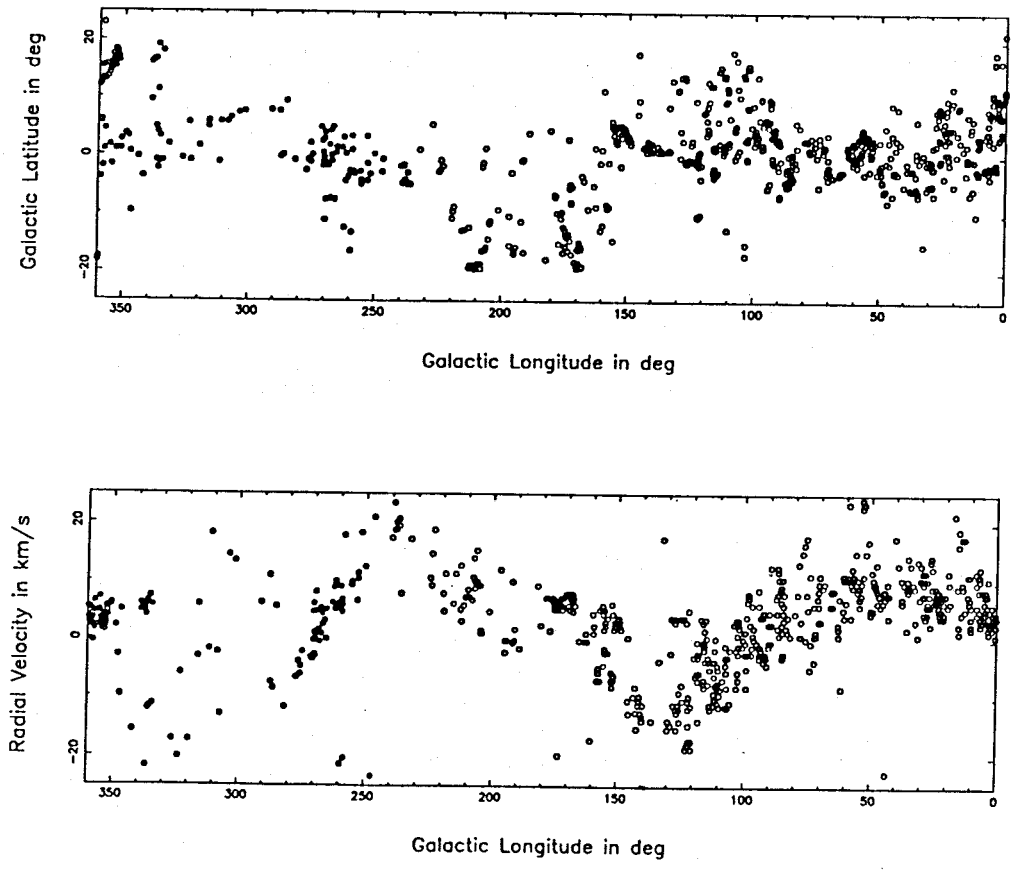

Fig.4.1 : Sky distribution of the local clouds is shown in (a) and the longitude-velocity plot in (b). Filled circles represent the southern clouds observed by us and the empty ones refer to the northern clouds detected by Taylor et al. (1987).

equation because most of the clouds have latitudes $|b| < 15°$ (Fig.4.1.b) making the correction unimportant.

The analysis procedure is broadly divided into three steps. In the directions close to the four longitudes 0, 90 180 and 270 degrees, the contributions of galactic differential rotation to the radial velocities of the local dark clouds are expected to be small. We refer to the longitude strips of width 18° centered around these four longitudes as "null directions". Thus, in these directions the observed velocities will be mainly due to systematic and peculiar components of non-circular motions. Hence the analysis of the clouds in these directions will enable us to reliably estimate the magnitude of these motions. This is done in section 4.2. As will be argued in that section the clouds in the "null directions" show clear evidence for expansion.

In section 4.3 we verify if this expansion is present in all the longitudes from an analysis of a subset of clouds with associated reflection nebulae. This is possible since their distances are known reasonably well. We also attempt a similar excercise on some specific local clouds identified in the CO surveys (Dame et al., 1987), which also have distance estimates. The clouds in this subset also show evidence of expansion.

In section 4.4 we turn to the analysis of the radial velocities of the general population of clouds distributed in all longitudes and derive estimates for their possible non-circular systematic velocities, the velocity dispersion of clouds and finally their spatial distribution.

Before we proceed, we wish to make the following remarks.

1. We shall consider each "condensation" of 1.5° extent in longitude and latitude, and 2 kms^{-1} width in velocity, as a *distinct kinematical entity*. The angular size was chosen to be 1.5° because at a distance of 400 pc, the mean distance of the dark clouds as suggested by Feitzinger and Stuwe (1986), the corresponding linear size would be 10 pc which is the upper end of the sizes of these dark clouds under study. Hence we convolved the measured points with a 3-dimensional gaussian of full width at half maximum in each of the three dimensions equal to the values mentioned above and picked all the local peaks. All points thus obtained are treated as "independent clouds" and used in the following analysis.

2. As we shall see, the velocities of the local clouds due to all causes turn out to be ~ 4 kms^{-1}. Thus, the few clouds with absolute velocities more than 25 kms^{-1} are likely to be far away and have been excluded from our analysis.

4.2 Clouds in the "null directions"

The first step in estimating the systematic velocities is to remove the effects of galactic differential rotation from the LSR velocities. In the four special directions

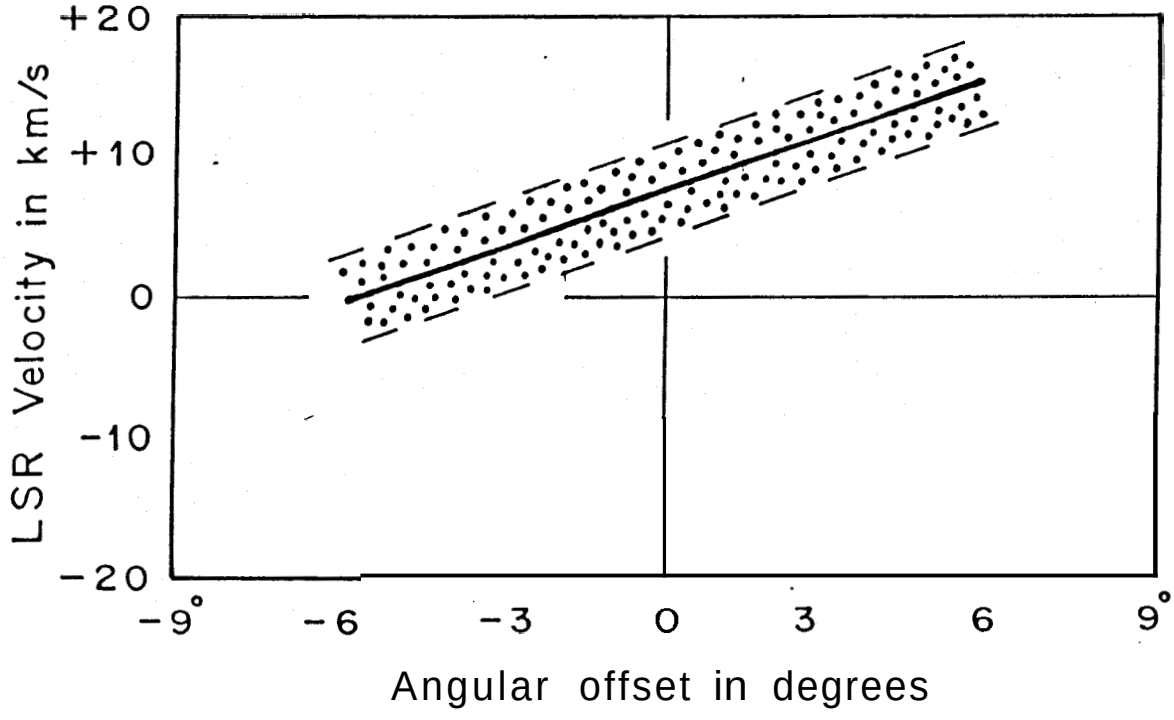

Fig.4.2 : A schematic diagram to illustrate the expected distribution of the LSR velocities around the 4 null directions. The slope of the distribution is a measure of the mean distances to the clouds, while the velocity distribution represents the width of the distribution. The mean systematic velocity if any will be given by the Y-intercept.

l_{II} = 0, 90, 180 and 270 degrees no such corrections need to be made for nearby objects, i.e. objects within, say, 1 kpc. To get a reasonable number of clouds in each of these directions we include all the clouds within a longitude strip of 18° centered around these directions in the present analysis. This width of 18° was chosen on the following basis: At the mean distance to these clouds of 400 pc as suggested by Feitzinger and Stuwe (1986), the maximum differential rotation contribution at the edges of the strip would only be ~ 2 kms^{-1}. If the clouds are evenly distributed about the central direction and even if the velocities are not corrected for these contributions, the resultant errors would only broaden the distribution and will not alter the mean. In any case we correct for the differential rotation contributions by adopting a mean distance to the clouds in each group based on the association of a few of the clouds with reflection nebulae. Distances thus obtained are also in reasonable agreement with estimates from the slopes of the distributions in longitude-velocity plots. The schematic shown in figure 4.2 illustrates this. The distribution of LSR velocities around any of these null directions would appear as a band with a slope, decided by the mean distance, a width due to the velocity dispersion of clouds and a Y-intercept giving the systematic velocity.

After correction for differential rotation on the above basis, only errors due to the dispersion in distances will be left over. Even if the dispersion in distance about the mean value is as much as the mean distance itself, i.e. $\sim$ 400 pc, the maximum error in the correction at either edge of the strip is ~ 1 kms^{-1} and the average error will be much less. Since this is comparable to the measurement errors in velocity and negligible compared to the dispersion velocities, taking the width of the longitude strip to be 18° is justified.

We have also removed very distant clouds from the sample within these longitude strips of 18°. Similarity in velocity and proximity on the sky to far away reflection nebulae (with reasonably good distance estimates) was the basis for such exclusion.

The sample of nearby clouds obtained as described above for each of the null directions was reasonably large. The LSR radial velocities were corrected for the differential rotation effects appropriate to their estimated average distances. The mean of these residual velocities gives the magnitude of the non-circular sytematic motions and the standard deviation gives the magnitude of the velocity dispersion of clouds. In the following subsections we give the details of the analysis for each of the null directions.

4.2.1 Galactic Centre Direction

Most of the reflection nebulae in the null direction about the galactic center are located at a mean distance of $\sim$ 150 pc which is the distance to the Ophiuchus group of dark clouds. However, one of them is located at 900 pc. The longitude-latitude distribution of clouds in this direction is shown in the figure 4.3.a. Their

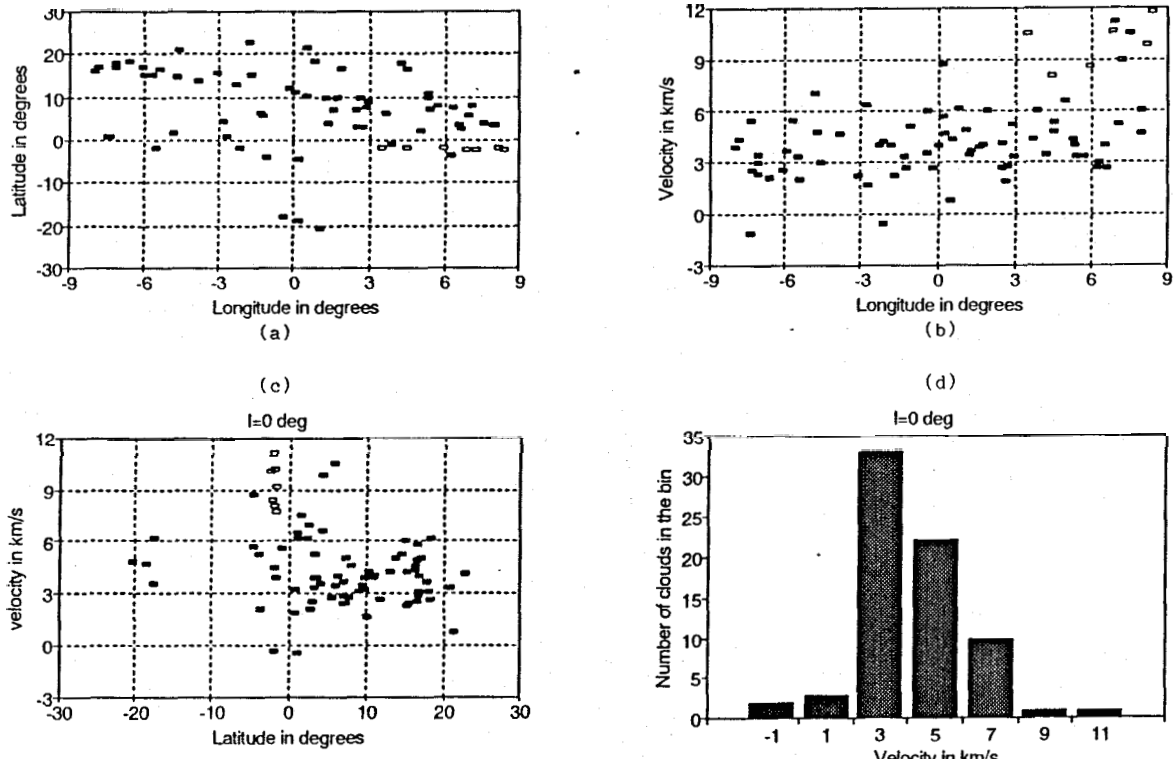

Fig.4.3 : The Galactic centre direction. The latitudes and LSR velocities of the clouds are plotted against their longitudes in (a) and (b), respectively. The group of clouds denoted by the empty rectangles are in a narrow range of longitude, latitude and velocity. Their most likely distance is $\sim$ 900 pc. Excluding this group from our sample the velocities of the rest of the clouds were corrected for differential rotation for an assumed distance of 180 pc. Fig.(c) shows the latitude-velocity plot, and a histogram of the residuals is shown in (d). Oort's A constant was taken to be 14.5 km/s/kpc.

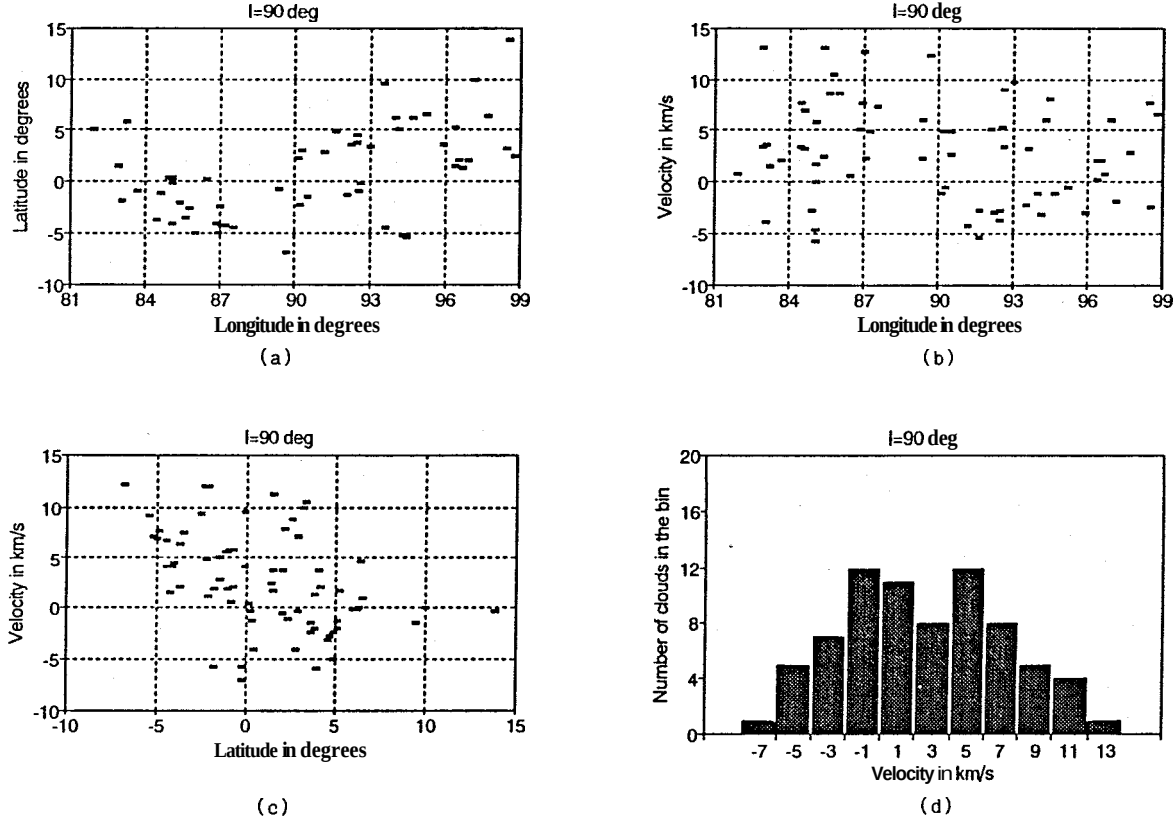

Fig.4.4 : l = 90° direction. The velocities have been corrected for an adopted distance of 500 pc for these clouds.

longitude-velocity distribution is shown in the figure 4.3.b. As seen in this figure a group of clouds, denoted by open squares, lying in the longitude range of 3° to 9° appear distinct with a mean velocity of $\sim$ 10.5 kms^{-1}. It can be seen from figure 4.3.a that they are also confined to a narrow range in latitude of $-1°$ to $-2.5°$. As one of these clouds is associated with a reflection nebula at 900 pc mentioned above, we have taken this sub-group of clouds to be not local, and excluded them from further analysis. For the rest of the clouds in this direction we adopt 180 pc as the mean distance. This is consistent with the slope of the distribution of clouds in the longitude velocity plot shown in figure 4.3.b being almost zero. In figure 4.3.c the residual velocities are plotted against latitude, and indicate that no latitude dependent motions exist. The histogram of the residual velocities is plotted in figure 4.3.d. A gaussian fit leads us to conclude that the clouds in this direction show clear evidence of recession with a velocity of 4.6 kms^{-1} and an rms dispersion of 2 kms^{-1}.

4.2.2 90° Longitude

In the null direction about 90° there are only four reflection nebulae. Of these, two are at a distance of $\sim$ 400 pc while the other two are at distances beyond 700 pc. The longitude latitude plot of the clouds in this direction is shown in figure 4.4.a. Notice the peculiar distribution of clouds in this direction. Their velocities are displayed against their longitude in figure 4.4.b and show a large dispersion. A straight line fit suggests a distance of 500 pc. Since we are unable to identify and remove distant clouds we adopt 500 pc to be the mean distance to them and correct the LSR velocities for the effects of differential rotation. In figure 4.4.c we display these residual velocities against the latitude. There appears to be a marginal linear correlation of velocity with latitude with a slope of 0.5 $kms^{-1}deg^{-1}$ which we do not consider significant. Figure 4.4.d shows the histogram of the resultant velocities. A gaussian fit leads us to conclude that the clouds in this null direction are also receding from us with a mean velocity of $\sim$ 2.7 kms^{-1} and an rms dispersion of $\sim$ 5 kms^{-1}.

4.2.3 180°Longitude

The reflection nebulae in this null direction about the anti- center longitude suggest that the clouds are mostly located at two distances: one at 130 pc corresponding to the Taurus group of clouds and the other at $\sim$ 350 pc. Figure 4.5.a shows the longitude-latitude plot of the clouds in this direction. The longitude-velocity plot is shown in figure 4.5.b. It is easy to identify the Taurus group of clouds which have LSR velocity more than 4 kms^{-1} and are located in the longitude range 165° to 180°. These are represented by the empty squares, We correct these clouds for differential rotation appropriate to a mean distance of 150 pc. We correct the rest of the clouds denoted by filled squares in the plots for a distnce of 350 pc.

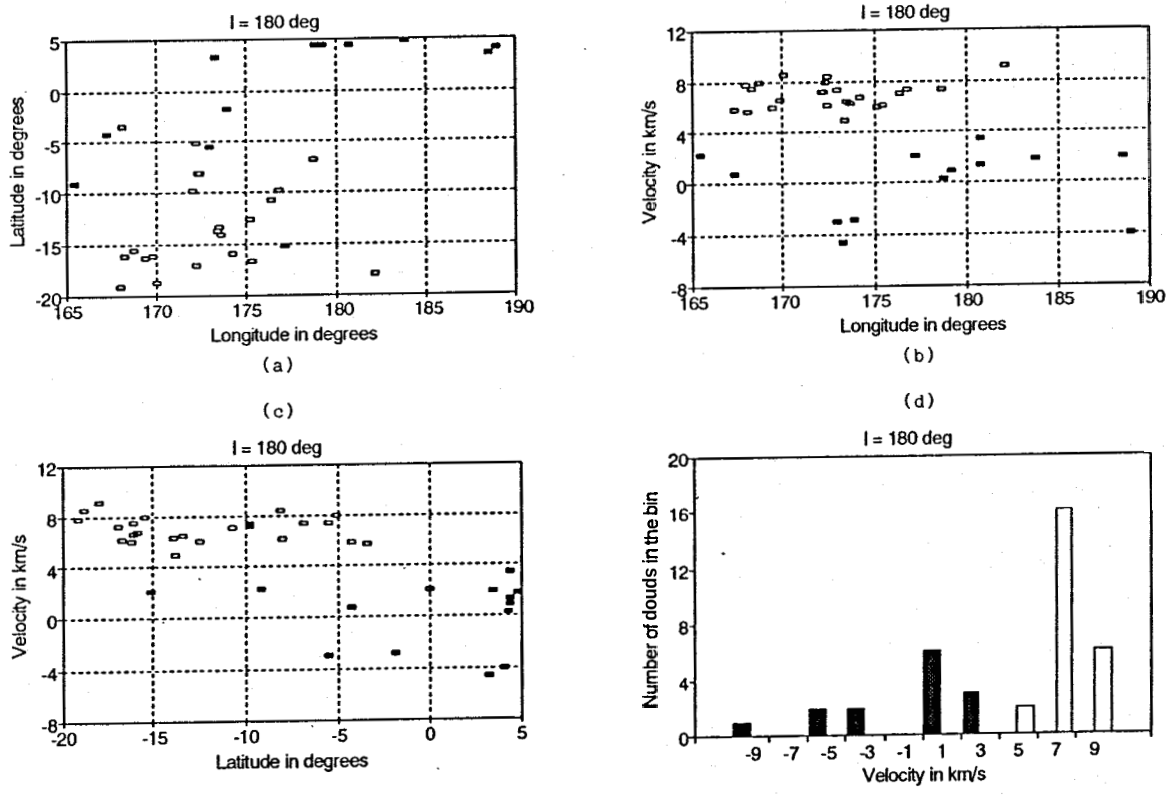

Fig.4.5 : $l = 180°$ direction. In these panels the open rectangles denote the Taurus group of clouds, and the rest are denoted by filled rectangles. While correcting for differential rotation a distance of 150 pc has been adopted for the Taurus clouds and 350 pc for the rest. The residual velocities are plotted in Fig.(c), and a histogram of these in Fig.(d).

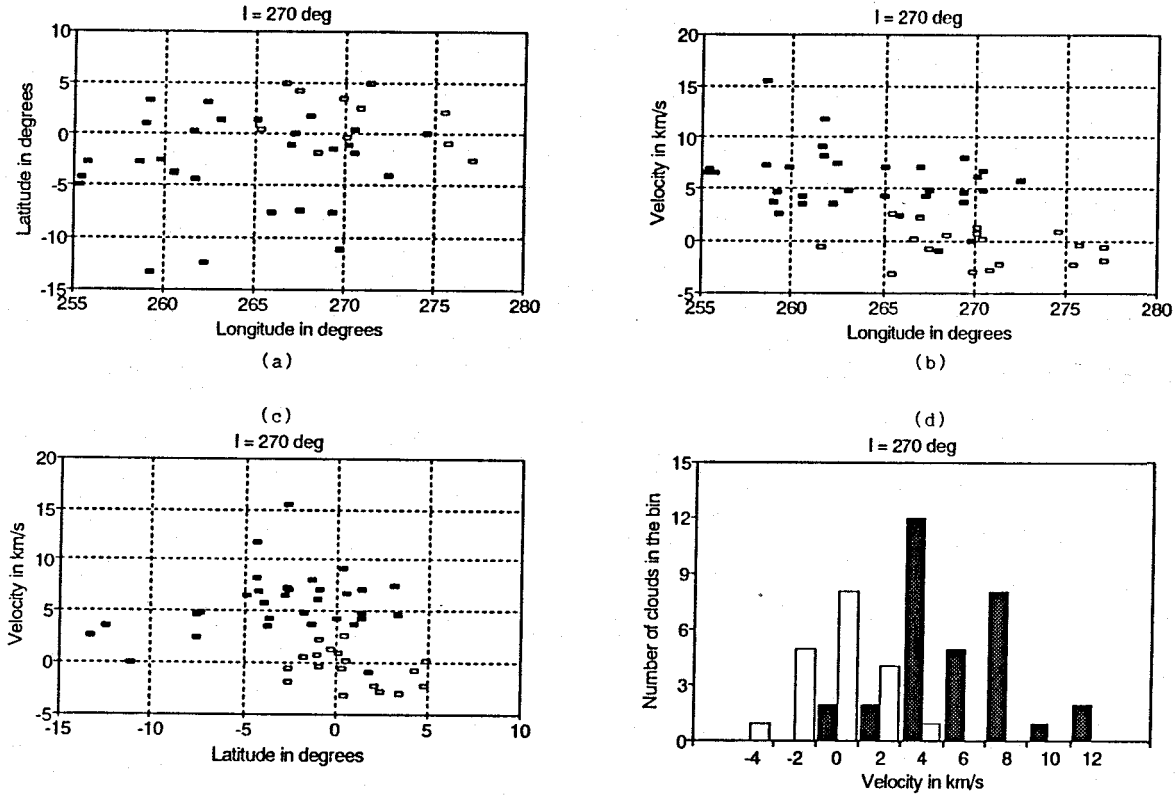

Fig.4.6 : l = 270° direction. The Vela Molecular Ridge clouds are denoted by open squares, and a distance of 1 kpc has been assumed for them. The others presumably associated with the Vela-IRAS shell have been assumed to be at 450 pc.

Figure 4.5.c shows the residual velocities plotted against the latitude. The distinct grouping of the Taurus clouds is clear. The histograms of the residual velocities for the two groups of clouds are shown in the figure 4.5.d. The Taurus clouds have an average velocity of 6.3 kms^{-1} and dispersion of 1.3 kms^{-1}. The other group of clouds have a mean of $\sim$ 0.3 kms^{-1} and an rms dispersion of $\sim$ 3.6 kms^{-1} dispersion. Hence we conclude that the nearer clouds in this direction belonging to the Taurus group show clear evidence for recession with a velocity of 6.3 kms^{-1} and a narrow dispersion of 1.3 kms^{-1}. There is no evidence of any systematic motions in the smaller number of clouds at 350 pc, while their dispersion is $\sim$ 3.6 kms^{-1}.

4.2.4 270° Longitude

In figure 4.6.a the latitudes are plotted against the longitudes for the clouds in the null direction about the 270° longitude. Their longitude-velocity plot is shown in figure 4.6.b. The slope of a linear fit to the entire sample implies a large distance of 2.1 kpc which is not substantiated by the reflection nebulae. Rather they indicate that there are two groups of clouds in this direction: one set of clouds belonging to the Vela Molecular Ridge (VMR) located at about 1 kpc and the other belonging to the Vela IRAS shell located at about 400 pc (Sahu, 1992). The large latitude extent of the clouds in the longitude range 255° to 270° suggests that the clouds in this direction are likely to be nearby. In the above plots the clouds likely to be associated with the VMR are represented by open squares and others by filled squares. We segregated the clouds into the two groups in the following manner: first we assigned all clouds within the longitude range of 265° to 280° and latitude range of -3° to 4° longitude to the VMR group and the rest to the Vela shell; then we corrected the assignments if the distances known to some clouds from associated reflection nebulae were not in accordance. Also three clouds falling within the above spatial boundary but having velocities very similar to the clouds that belong to the Vela IRAS shell were also grouped with them. We believe that the separation is reasonably successful from the fact that the filled squares clearly trace the Vela IRAS shell in the sky. Also, separate linear fits to the LSR velocities of the clouds assigned to VMR and Vela IRAS shell indicated distances of 1.1 kpc and 550 pc respectively supporting the separation into two groups. However, we correct the clouds belonging to the Vela IRAS shell for differential rotation appropriate to a distance of 400 pc, given by the reflection nebula and supported by Sahu (1992). The clouds belonging to VMR are corrected for a distance of lkpc. The residual velocities are plotted against latitude in figure 4.6.c. The histogram of the residual velocities is shown in figure 4.6.d. The VMR clouds represented by the empty rectangles show a nearly zero mean velocity and an rms dispersion of 1.5 kms^{-1}. The clouds associated with the Vela IRAS shell are represented by the filled rectangles. They show a mean of $\sim$ 6.5 kms^{-1} and an rms deviation of 3 kms^{-1}. Hence we conclude that the clouds located at 400 pc in the null direction

around 270° also show clear evidence for recession with a velocity of $\sim$ 6.5 kms^{-1} and a random velocity dispersion of 3 kms^{-1}.

Summary of the results from the null directions analysis:

We conclude that the above analysis of LSR velocities from clouds in the null directions clearly demonstrates that receding motions of 3 to 6 kms^{-1} are present in all of them. The magnitude of the velocity dispersion of clouds is $\sim$ 2.5 to 5 kms^{-1}. These are much lower than 7 to 10 kms^{-1} derived by Stark (1984). We discuss this in Section 5.5.2. The following table summarises the results obtained in this section.

Table 4.1 : Results of *null* direction analysis.

LONG	v_{exp}	a	Comments
0	4.6	2.0	Ophiuchusgroupofclouds]
90	2.7	5.0	
180	6.3	1.3	Taurus group of clouds
270	6.5	3.0	Vela IRAS shell

4.3 Clouds with known distances

In the previous section we found that the system of clouds in all the four null directions are clearly receding from us. In this section we wish to verify whether this applies more generally in other directions as well by'studying a subset of clouds for which there are reasonably good distance estimates. We use two sets of clouds:

1. The first group consists of molecular clouds with associated reflection nebulae (both southern and northern clouds). Their distances are from Racine (1968), and van den Bergh and Herbst (1975). Their velocities are from Kutner et al. (1980), de Vries et al. (1984), and our present work.

2. The second set of clouds are those identified by Dame et al. (1987) as "individual". We shall adopt distances suggested by them.

4.3.1 Clouds with associated reflection nebulae

Reflection nebulae arise when there is a bright star (usually a B star) close to a molecular cloud. This enables one to estimate the distances to such clouds from a determination of the distances to the exciting stars. Estimating stellar distances involves measuring the apparent visual magnitude (V) and estimating the absolute visual magnitude and the visual extinction. Visual extinction (A,) is taken to be three times the B − V colour excess E(B − V) (Blanco, 1956). This colour excess is directly measured or computed from the intrinsic colours derived from the MK spectral types. Stellar spectra are classified on the MK system comparing the $H\gamma$

Table 4.2 : Reflection Nebulae within 500pc.

Source	l deg	b deg	Dist kpc	V_{LSR} kms^{-1}	V_{res} kms^{-1}	Source	l deg	b deg	Dist kpc	V_{LSR} kms^{-1}	V_{res} kms^{-1}
nrn124	21.0	–0.5	0.17	6.9	5.3	**nrn031**	172.5	–0.8	0.12	6.2	6.7
nrn123	31.6	5.2	0.44	7.2	1.5	**nrn041**	182.5	–5.9	0.16	7.7	7.5
nrn129	41.6	–18.1	0.04	0.1	–0.5	**nrn056**	190.5	–6.9	0.26	8.9	7.5
nrn126	57.0	3.0	0.48	11.7	5.3	**nrn038**	194.6	–15.6	0.32	0.5	–1.8
nrn135	73.5	–5.1	0.35	12.4	9.6	**nrn040**	196.8	–15.7	0.24	–5.4	–7.3
nrn136	81.4	0.5	0.40	8.5	6.8	**nrn043**	198.1	–14.6	0.38	–10.3	–13.6
nrn147	94.3	–5.3	0.44	6.7	7.7	**nrn044**	207.8	–19.7	0.55	**11.1**	4.5
nrn152	110.3	11.4	0.40	–5.3	–1.5	**nrn055**	212.4	–19.0	0.38	2.7	–2.3
nrn158	110.6	–12.6	0.48	–8.1	–3.5	**nrn087a**	221.8	–2.0	0.50	39.8	32.6
nrn150	111.9	14.1	0.50	–4.0	1.0	**nrn086**	222.7	–3.4	0.42	11.9	5.8
nrn003	121.4	6.6	0.18	–6.8	–4.5	**nrn090a**	224.4	–2.7	0.52	14.1	6.6
nrn007	132.9	9.1	0.08	–13.3	–12.1	**nrn098**	240.4	–2.2	0.38	23.0	18.3
nrn008	133.9	7.6	0.21	–11.6	–8.6	**srn10a**	259.3	–3.8	0.48	8.9	6.4
nrn012	157.4	–20.6	0.17	**1.1**	2.8	**srn28**	265.1	1.4	0.50	5.2	4.0
nrn013	158.0	–21.3	0.29	7.0	9.9	**srn12**	266.2	–7.8	0.48	3.3	2.4
nrn017	158.3	–20.4	0.50	7.2	12.2	**srn23**	267.0	–0.9	0.46	4.5	3.8
nrn016	159.2	–21.9	0.14	5.3	6.6	**srn63**	314.9	–5.1	0.42	4.8	10.9
nrn019	160.5	–17.8	0.30	8.6	11.3	**nrn105**	352.9	17.0	0.17	3.6	4.2
nrn032	162.5	1.5	0.30	–2.4	0.1	**nrn108**	353.1	15.9	0.14	4.5	5.0
nrn025	171.4	–19.8	0.11	**11.1**	11.6	**nrn106**	353.7	17.7	0.14	2.3	2.7
nrn029	172.1	–9.7	0.15	6.4	7.0	**nrn100a**	354.6	22.7	0.15	5.1	5.5
nrn034	172.1	–2.3	0.32	6.8	8.1	**nrn102x**	355.5	20.9	0.13	3.3	3.6

Table 4.2 (...contd.) : Reflection Nebulae outside 500pc

Source	l deg	b deg	Dist kpc	V_{LSR} kms^{-1}	V_{res} kms^{-1}	Source	l deg	b deg	Dist kpc	V_{LSR} kms^{-1}	V_{res} kms^{-1}
nrn115	7.4	−1.8	0.91	8.9	5.5	nrn080a	219.3	−9.0	0.76	12.6	1.8
nrn128	69.5	0.4	0.83	−2.2	−10.1	nrn093	223.7	−1.9	0.72	17.9	7.5
nrn131x	80.5	2.7	1.05	5.0	0.0	nrn095	224.7	−1.8	0.79	15.6	4.1
nrn142	99.1	3.9	0.72	−8.2	−4.9	nrn094	225.5	−2.6	0.83	12.4	0.4
nrn155	109.6	2.4	0.58	−9.5	−4.2	srn05	253.1	−1.4	1.32	10.4	−0.2
nrn001c	117.3	−3.7	0.52	−11.4	−5.3	srn03	255.5	−4.2	1.15	9.9	1.8
nrn002	119.0	3.0	0.63	−19.5	−11.8	srn04	255.6	−3.0	0.87	8.9	2.8
nrn014	141.5	2.9	0.76	7.6	18.3	srn17	260.0	−0.1	0.95	7.8	3.1
nrn039	174.3	−1.7	0.72	7.4	9.5	srn27	264.3	1.9	0.91	7.0	4.4
nrn047	184.0	−4.2	0.87	3.0	1.2	srn25b	264.4	1.4	0.60	6.3	4.6
nrn075	188.7	3.8	0.55	3.0	0.6	srn29	268.0	1.8	0.79	−0.5	−1.3
nrn077x	201.9	0.0	1.00	0.0	−10.0	srn30	270.8	0.8	0.95	6.9	7.3
nrn051	206.0	−16.3	0.66	9.8	2.3	srn72	336.4	−1.4	1.38	−12.4	2.3
nrn057	207.1	−16.2	0.58	9.8	3.0	srn92	358.5	−2.1	1.32	−0.5	0.5
nrn068x	213.7	−12.4	0.76	9.5	−0.7						

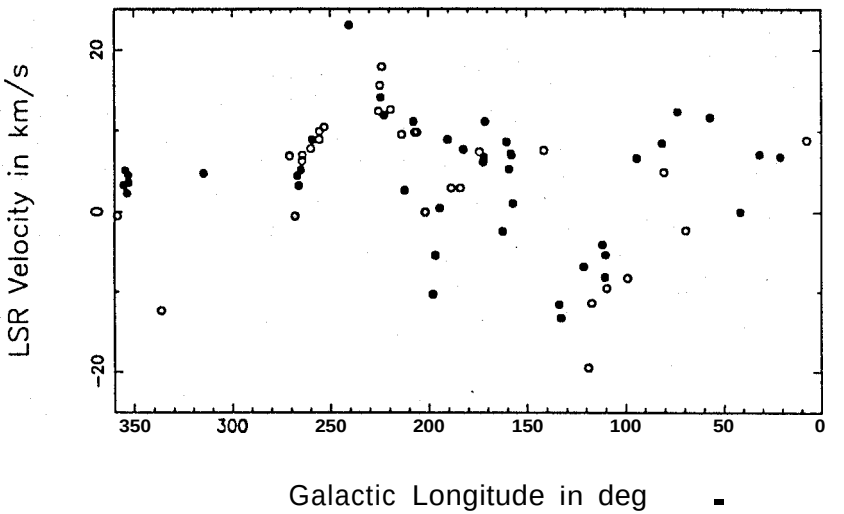

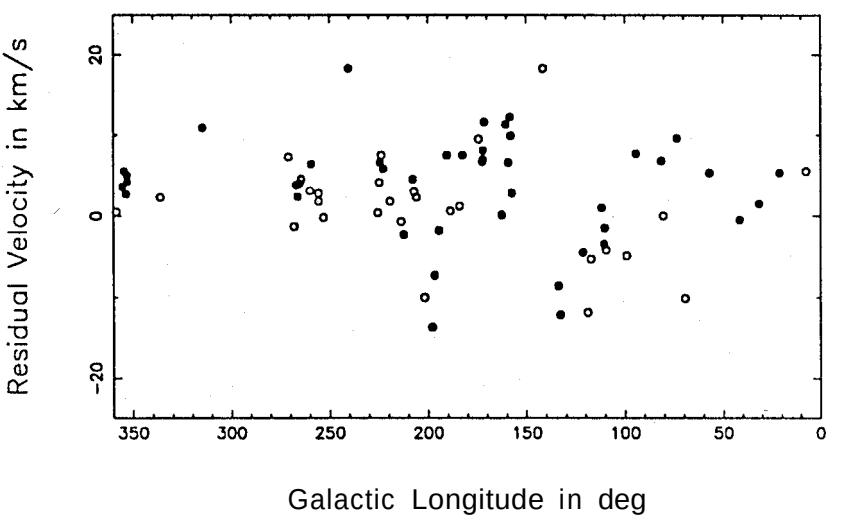

Fig.4.7 : **LSR** velocities and the residual velocities of clouds with associated reflection nebulae are shown against their longitudes in (a) and (b) respectively. The filled circles represent clouds within 500 pc, and the empty ones represent clouds which are beyond 500 pc.

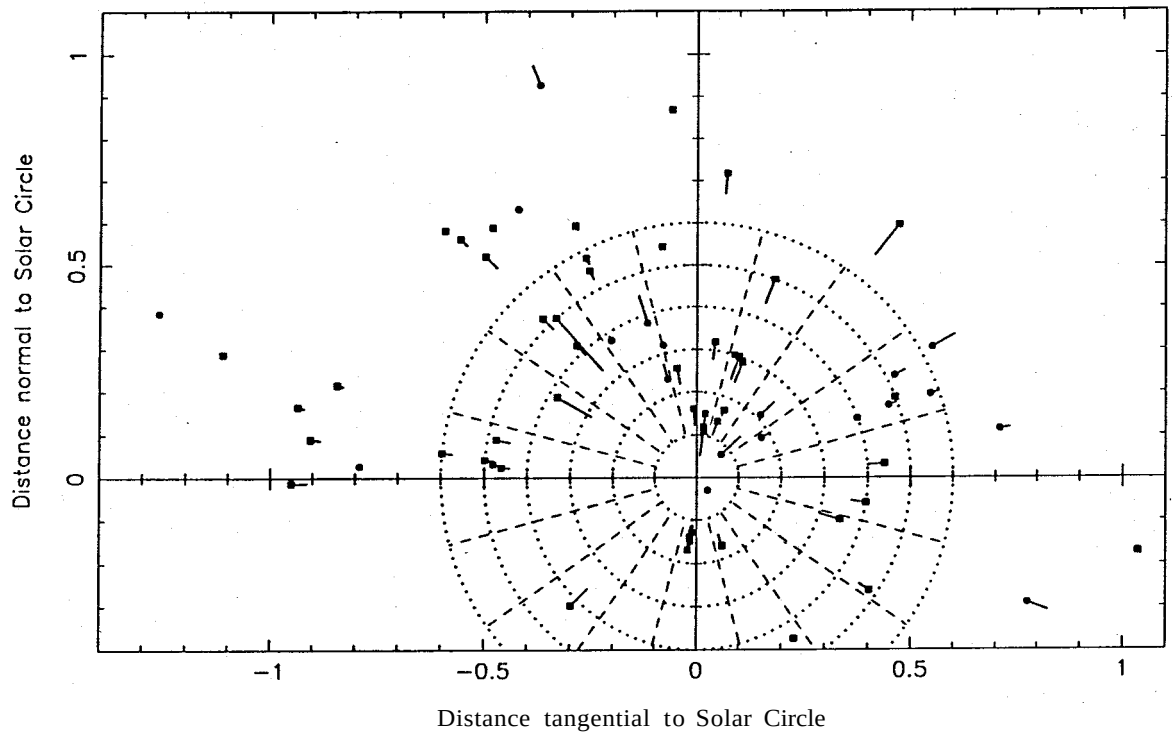

Fig.4.8 : The spatial distribution of clouds with reflection nebulae projected onto the galactic plane. The mid-points of the *tadpoles* indicate the position of the clouds, while the lengths of the *tails* indicate the magnitude of their velocities. Clouds with outward radial velocities are indicated by squares, and those coming in by filled circles. The Sun is located at the centre of the system of concentric circles. Notice that the clouds in the longitude ranges 100° – 145" and 195° – 215° are predominantly coming in.

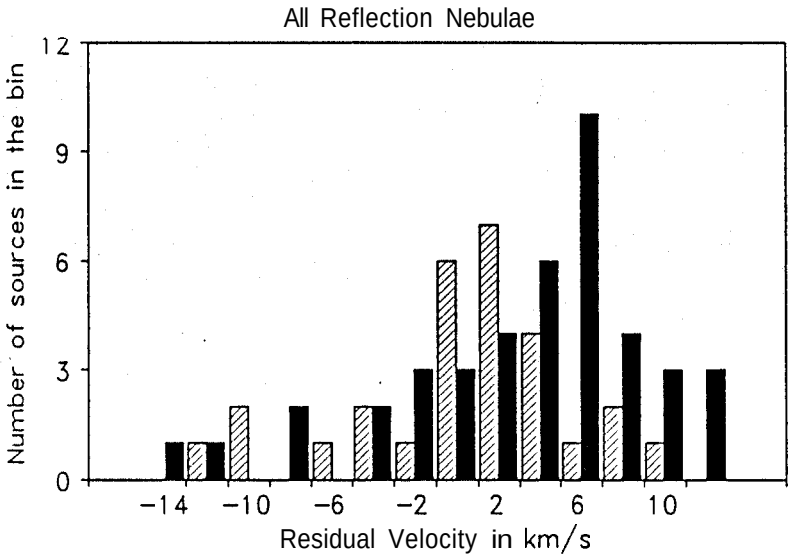

Fig.4.9.a : A histogram of the residual velocities of clouds with reflection nebulae. Clouds within 500 pc are denoted by filled bars, while those beyond 500 pc are denoted by hatched bars.

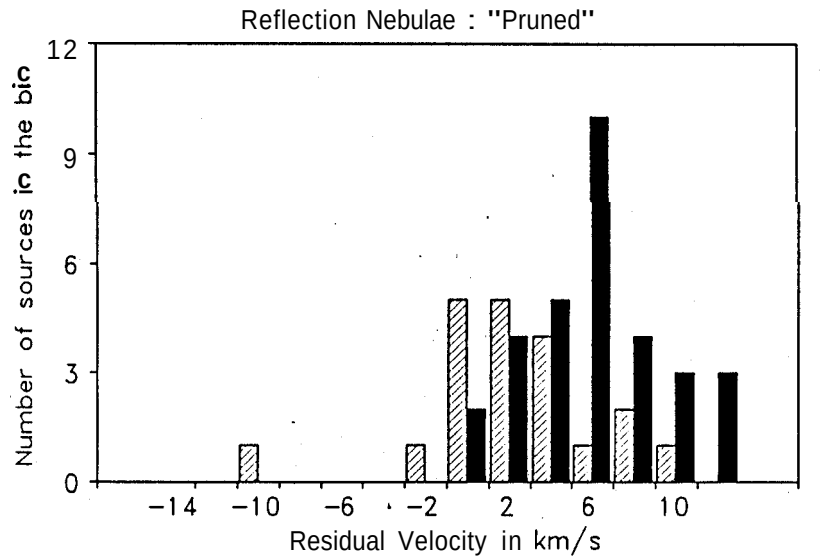

Fig.4.9.b : A histogram similar to Fig.(a) but excluding all clouds in the longitude ranges 100° − 145° and 195° − 215°, i.e. excluding clouds that are corning in.

width of the program stars with those of some standard calibration stars, also measured along with the program stars. The absolute visual magnitudes (M_v) are obtained either using the $H\gamma$ width as calibrated by Petrie (1965) or the photometrically determined $(U-B)_0$ colours calibrated against the absolute magnitudes of corresponding spectral type (Schmidt-Kaler, 1965). The distance modulus is then $V - M_v + A_v$. Generally UBV photometry and Hy spectrometry are done to obtain the distances. Racine (1968) has obtained the distances to the northern reflection nebulae while van den Bergh and Herbst (1975) have obtained distances for the southern ones. The quantities relevant to our discussion, taken from the literature, are summarized in Table 4.2. It lists the clouds with associated reflection nebulae, both northern and southern, their longitudes, latitudes, distances and LSR velocities.

In figure 4.7.a we have displayed their velocities and longitudes. The filled squares represent LSR velocities of clouds within 500 pc while the empty squares refer to the clouds beyond 500 pc. There are 44 clouds within 500 pc and 29 beyond. In figure 4.7.b the residual velocities after removing the contributions due to the galactic differential rotation are plotted following the same convention for the symbols. Figure 4.8 shows the spatial distribution of the residual velocities of the clouds projected onto the plane of the galaxy with the Sun at the origin and the galactic center towards the negative Y-axis. Notice that in the longitude ranges 100° to 145° and possibly 195° to 215° the clouds predominantly show incoming velocities. Figure 4.9.a shows a histogram of these residual velocities. The filled rectangles represent the clouds within 500 pc, while the empty ones refer to the clouds beyond. The clouds within 500 pc show a clear trend of expansion with a mean velocity of ~ 4.3 kms^{-1}. However there is a large apparent dispersion. Clouds outside 500 pc show only marginal evidence for expansion. The clouds in the longitude ranges 100° to 145°, and 195° to 215° form a distinct kinematical group, with predominantly negative (inward) velocities. They have the effect of reducing the mean expansion velocity and increasing the apparent dispersion. The distribution of the residual velocities after removing these two sectors is shown in figure 4.9.b. The same convention is used as before to indicate the clouds within 500 pc and beyond. After the removal there are 33 clouds within 500 pc and 20 beyond. The expansion velocity for the clouds within 500 pc is 7.2 kms^{-1} with a standard deviation for the random velocities of 5.8 kms^{-1}. Clouds outside 500 pc also show a marginal expansion of 2.3 kms^{-1} with 4 kms^{-1} random velocity dispersion.

To summarize, the kinematical analysis of the clouds with associated reflection nebulae within 500 pc of Sun confirms that expansion is present in all longitudes except the longitude ranges 100°-145° and 195°-215°. These longitudes are dominated by clouds with incoming peculiar motions. The mean expansion velocity in other longitudes is 7.2 kms^{-1} with a dispersion of 5.8 kms^{-1}.

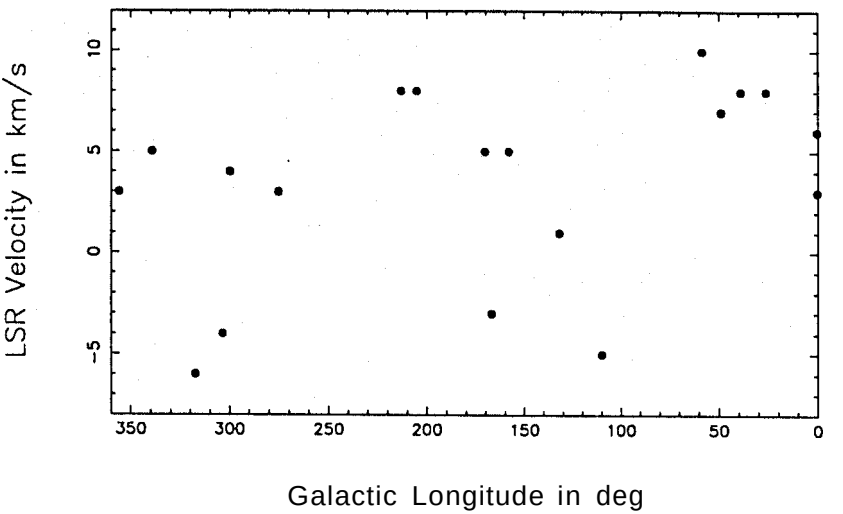

Fig.4.10.a : The LSR velocities of clouds within 500 pc identified from the composite CO survey by Dame et al. (1987).

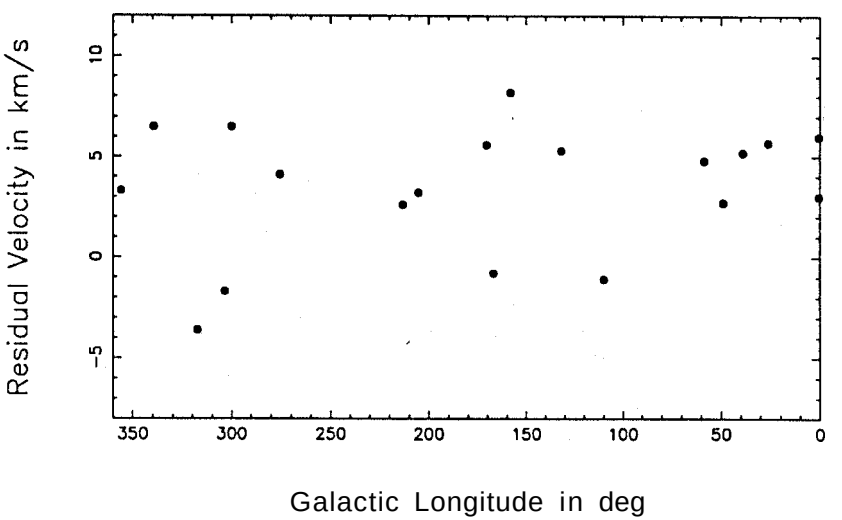

Fig.4.10.b : A plot of the residual velocities after correcting for differential rotation assuming distances suggested by Dame et al..

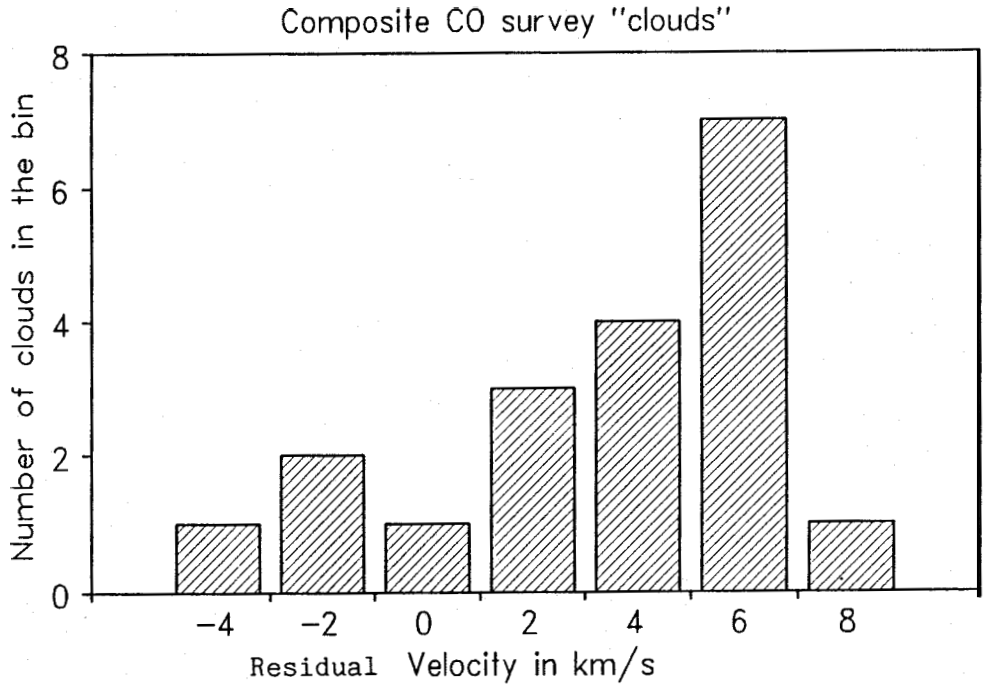

Fig.4.11 : A histogram of the residual velocities of the CO survey clouds.

4.3.2 Clouds identified from composite CO survey

Dame et al. (1987) have identified clouds and cloud complexes within 1 kpc from the composite CO survey. In general, these complexes have large angular extent. In Table 2 of their paper, Dame et al. have listed these clouds, their longitude and latitude ranges, their measured radial velocities and their distances compiled from the literature. These distances are based on associated Population I objects or on star counts or on the relation of visual absorption to distance for stars within the cloud boundary. Here we analyze the radial velocities of clouds within 500 pc. The quantities relevant to our discussion are summarized in Table 4.3. We have used 8 kms^{-1} and 3 kms^{-1} as the velocities of the Orion and Vela clouds respectively. The longitudes and latitudes listed in our Table are the averages of the boundary values given by Dame et al..

Table **4.3** : Composite CO survey clouds.

Source	lII°	bII°	$V_{LSR}(\mathrm{kms}^{-1})$	Dist.(kpc)	$V_{res}(\mathrm{kms}^{-1})$
ρ Ophiuchus	0.5	7.8	3.0	165	3.0
R CrA	0.5	−18.0	6.0	150	6.0
Aquila rift	26.3	2.0	8.0	200	5.7
Aquila rift	39.0	0.0	8.0	200	5.2
Cloud B	49.0	0.5	7.0	300	2.7
Vulpecula rift	58.5	1.0	10.0	400	4.8
Cepheus	110.0	16.5	−5.0	450	−1.1
Lindblad ring	132.0	3.0	1.0	300	5.3
Perseus 2b	158.3	−16.0	5.0	350	8.2
Perseus 2a	167.0	−7.5	−3.0	350	−0.8
Taurus	170.5	−15.8	5.0	140	5.6
Orion B	205.3	−13.5	8.0	450	3.2
Orion A	213.3	−17.8	8.0	450	2.6
Vela sheet	275.5	2.5	3.0	400	4.1
Chamaleon	300.0	−16.0	4.0	215	6.5
Coal sack	303.5	−0.5	−4.0	175	−1.7
G317−4	317.5	−4.0	−6.0	170	−3.6
Lupus	339.5	13.0	5.0	170	6.5
ρ Ophiuchus	356.0	18.5	3.0	165	3.3

The longitude-LSR velocity plot of these clouds is shown in Fig.4.10.a. The residual velocities corrected for differential rotation appropriate to the distances are shown in Fig.4.10.b. As seen in the figure all except 4 clouds (G317-4, Coalsack, PerOB2b and Cepheus) are receding from us. A histogram of the residual velocities is shown in figure 4.11. The mean velocity of expansion is $\sim$ 3.5 kms^{-1}, with a velocity dispersion of clouds of $\sim$ 3 kms^{-1}. We realise that these "clouds" have large spatial extent and any analysis which assigns a single position, distance and LSR velocity (as done here) is bound to be inaccurate. It is significant that this

analysis leads us to the same conclusions as before, viz. that the local clouds are in a state of expansion in spite of the scatter introduced by this assumption.

4.4 The general population of clouds

So far we have demonstrated that a subset of clouds distributed over the entire longitude range show evidence of expansion of about 3 to 5 kms^{-1}. There is a velocity dispersion of clouds of 2.5 kms^{-1} to 5 kms^{-1} depending upon the longitude. In the present section we attempt to establish whether this apparent expansion about a common center is true for the entire population of the local clouds (The radial velocities for the northern clouds are from Taylor et al. (1987) and for the southern clouds are from the present work). We also wish to derive a model describing the spatial distribution of these local dark clouds. We do this by a Monte-Carlo simulation and by comparing the cumulative distributions of the simulated population with those of the observed population. Before describing this procedure the following remarks are needed. In each of the four quadrants in longitude we exclude clouds within 15° from the null directions since there is not much distance information that can be derived in these directions. Thus, within each quadrant only clouds within the central 60° are considered. In the first 3 quadrants these 60° segments are further divided into three sectors of 20° each. However since the total number of clouds in the fourth quadrant is only 25 (if one excludes the more distant ones), we analyse them as one single group. Thus the sample included in the analysis of this section is divided into 10 groups. Now we describe the analysis procedure.

4.4.1 Analysis Procedure

Our basic model is that the local population of dark clouds can be described by an expanding doughnut-shaped configuration with well defined inner and outer radii. In the anaysis to follow we shall be merely concerned with the projection of such an assumed configuration onto the galactic plane. We shall further assume that the clouds are distributed within this doughnut in such a manner that the areal density of clouds is a constant. Consider a particular sector bounded by the longitudes $l1$ and 12. Let n be the number of observed clouds in this sector. The only observational input is their measured LSR radial velocities. Let us assume for a moment that the observed radial velocities are purely due to galactic rotation. One can then compute the corresponding kinematic distances using the expression

$$V_{rot}(l) = AD_{kin}\sin(2l) \tag{4.2}$$

where A is Oort's constant which is taken to be 14.5 $\mathrm{kms}^{-1}\mathrm{kpc}^{-1}$. Next we construct a cumulative distribution of these kinematical distances i.e. $\mathrm{N}(< D_{kin})$ vs D_{kin}. We then compare this cumulative distribution with that of a simulated

population distributed according to the model described above. This is done as follows:

Step 1 : For a particular sector we generate a model population within the section of the doughnut consisting of the same number of clouds as the observed population. The clouds are distributed at random within the longitude sector keeping the areal density constant. Every cloud within this sector is assigned a radial velocity arising out of galactic differential rotation, appropriate to its randomly chosen location within the sector (i.e. its distance from us and its specific longitude). In addition there will be a contribution to the radial velocity due to its non-circular systematic motion, V_{sys}, as well as a radial component due to peculiar or random motions. These random velocities are assumed to have a Gaussian distribution with a well defined velocity dispersion. Thus, the radial velocity of any cloud in the simulated population can be written as

$$V_{rad}(l) = Ad \sin 2l + V_{sys} + V_{pec} \tag{4.3}$$

To summarize, the various parameters that enter our model are : (i) the inner and outer radii of the annulus: R_l and R_h (ii) the systematic velocity : V_{sys} (iii) the dispersion in velocity : a.

Step 2 : We next convert the net radial velocities of each cloud to a kinematical distance (by assuming that the net velocity is entirely due to "galactic differential rotation" as was done for the true population) and construct a cumulative distribution of these kinematical distances. Since the number of clouds in the simulated population is rather small (typically ~ 25 in a given sector) before comparing such a cumulative distribution we derive an "ensemble-averaged cumulative distribution" by repeating the simulations 50 times using a different seed number each time. Finally, it is this ensemble-averaged cumulative distribution derived for a particular set of values for the parameters of the model that we compare with the observed distribution.

Step 3 : As mentioned above, in obtaining the cumulative distribution for the simulated population one has assumed a particular set of values for the non-circular systematic velocity, velocity dispersion, and the distances to the inner and outer radii of the annulus in that direction. The procedure is now repeated by assuming different sets of values for the parameters mentioned above and choosing the "most probable" set of values depending upon which combination best reproduces the observed cumulative distribution. We compare the observed and simulated distributions using the Kolomogorov-Smirnov test. Since there are in principle four parameters, we use a partly sequential search as described below:

(a) To begin with, the dispersion in peculiar or random velocities (a) was fixed at a value determined from the earlier analysis of the clouds along the four null directions (Section **4.2).** It may be recalled that the dispersion in the peculiar

Caption for Figures 4.12 to 4.21

These figures show the cumulative distribution of the *kinematic distances* of the observed clouds and those of the simulated populations for each of the ten longitude sectors. The filled circles represent the observed clouds, and the continuous line is the ensembled-averaged cumulative distribution of the simulated populations. For each of these longitude directions the fits have been shown for two different Kolmogorov and Smirnov probabilities. The parameters for the good and somewhat poorer fits are given in Table 4.4. The probabilities take discrete values owing to the smallness of the sample. Hence 100% probability for a set of parameters does not mean certainty but rather that they are highly probable. The parameters derived for the various longitudes are self-consistent and are also in good agreement with our other analyses as well as with other evidences such as the distribution of the local dust complexes (Lucke, 1978) derived from the reddening measurements. Hence the derived information is not likely to be contaminated by fitting the noise.

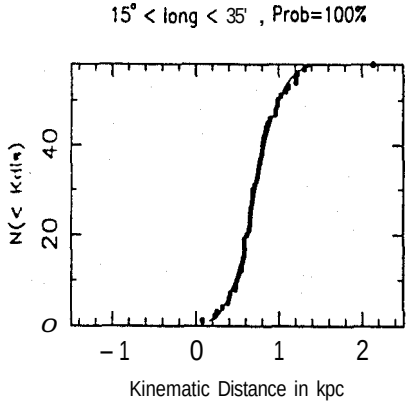

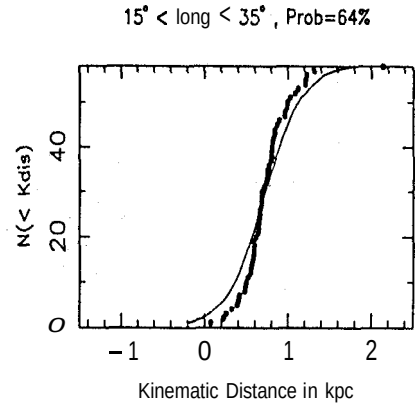

FIG. 4.12 .

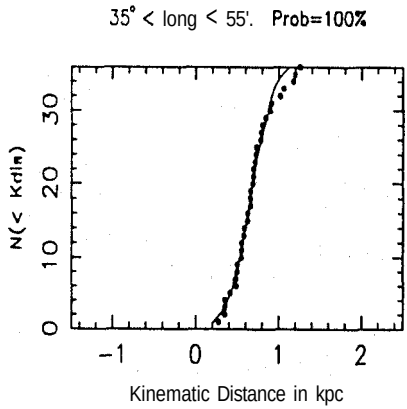

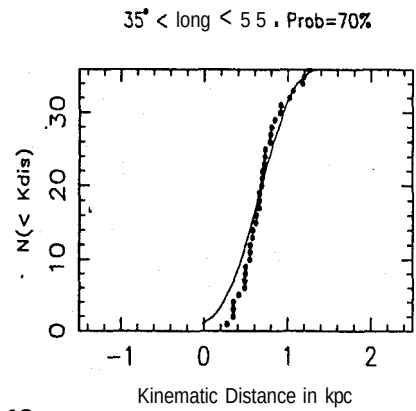

FIG. 4.13

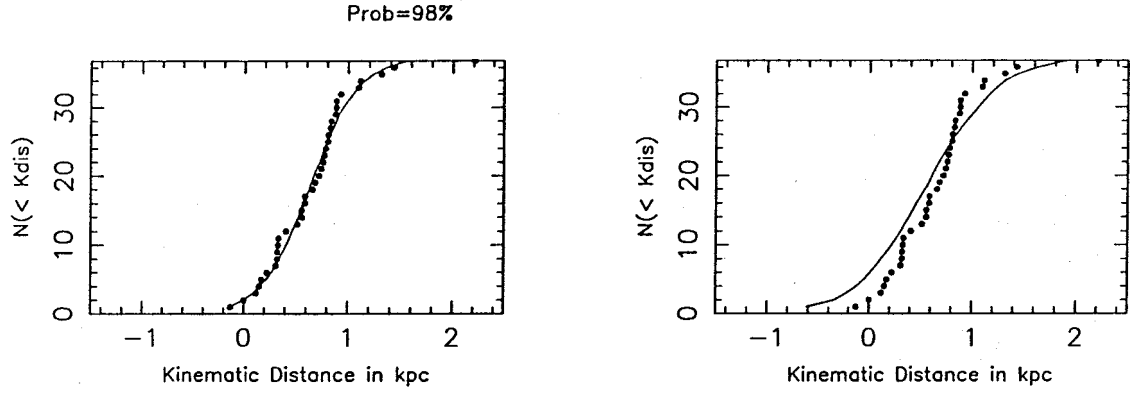

FIG. 4.14

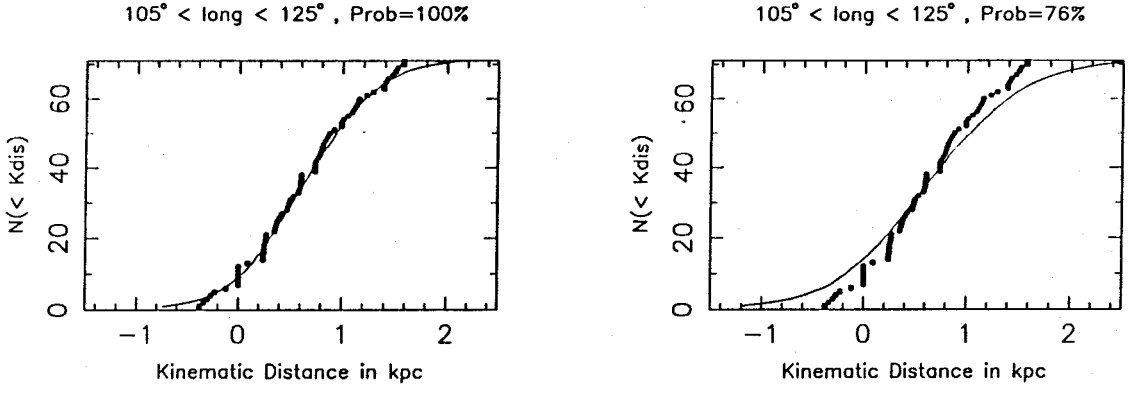

FIG. 4.15

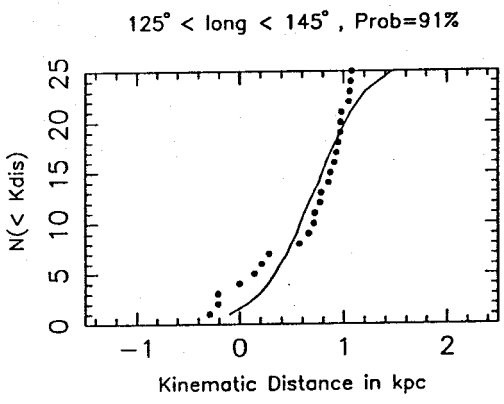

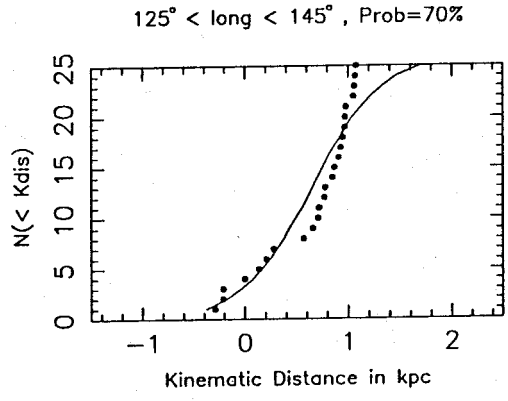

Fig. 4.16

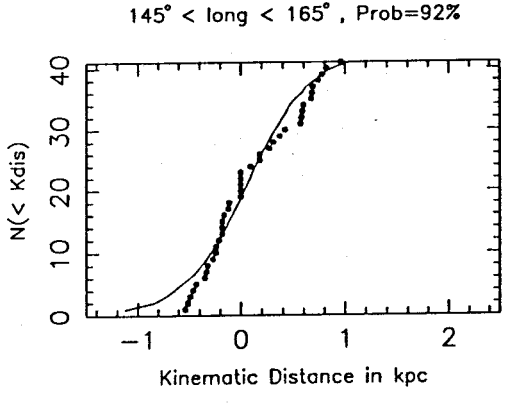

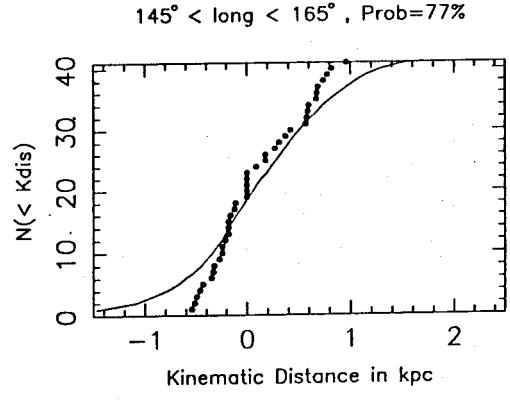

Fig. 4.17

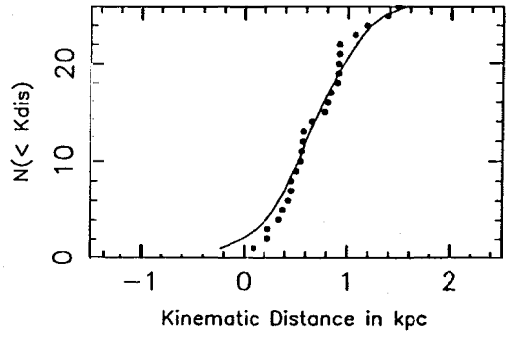

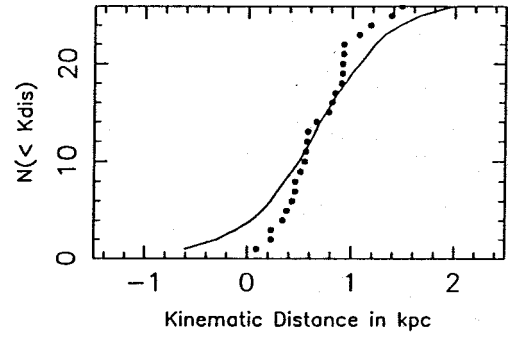

Fig. 4.18

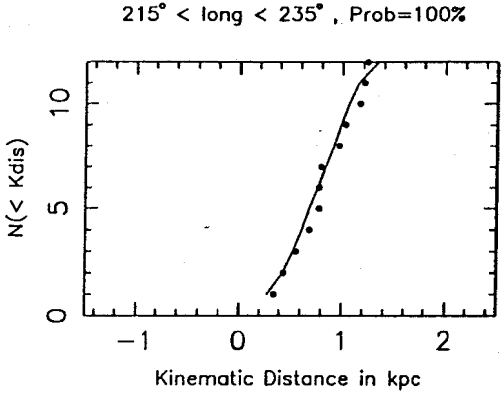

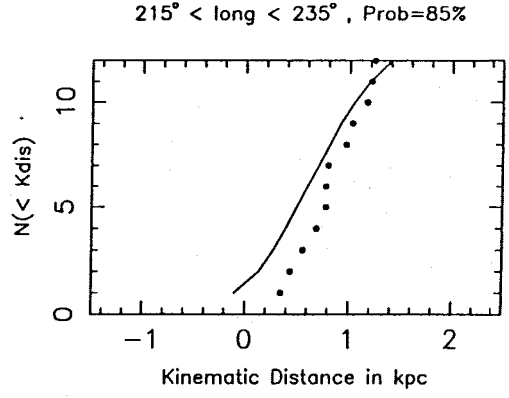

Fig. 4.19.

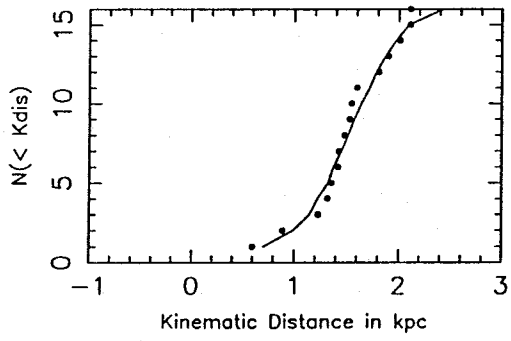

Prob=70%

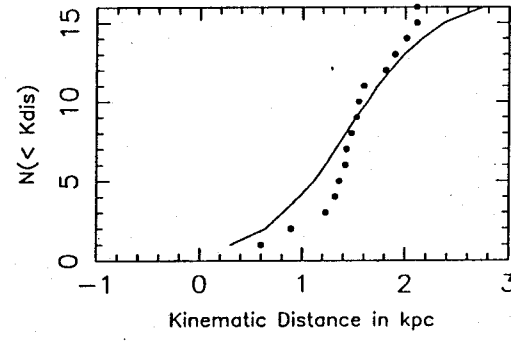

Fig. 4.20

285° < long < 345° , Prob=100%

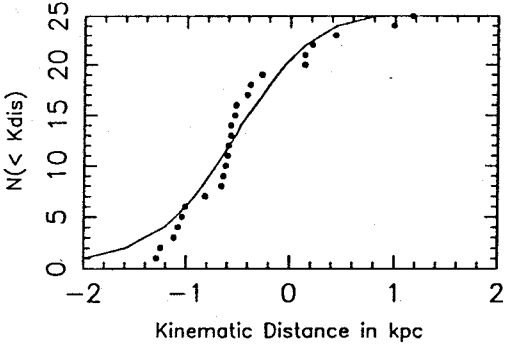

285° < long < 345° , Prob=70%

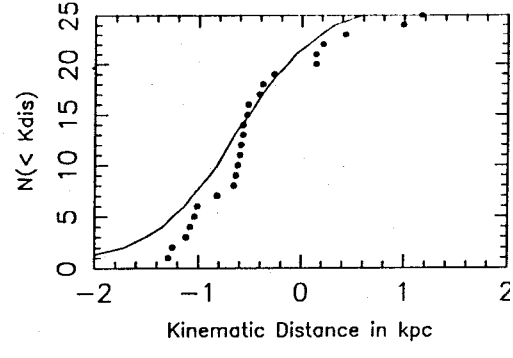

Fig. 4.21

velocities varied from 2.5 to 5 kms^{-1} depending on the direction. The velocity dispersion in any particular direction was obtained by interpolation.

The non-circular systematic velocity, inner and outer radii of the annulus as measured from the Sun were varied and the cumulative distributions were compared with that of the observed sample (refer to "step 2" described above). The best-fit distribution was identified as the one with the highest Kolomogorov-Smirnov probability. Thus, for every given longitude sector the most probable values for V_{sys}, R_l and R_h were obtained. The variation of the K-S probabilities with respect to these parameters was not strongly peaked and therefore the derived parameters could not be sharply fixed. When summarising the results of our simulations in Appendix D at the end of this thesis we shall ascribe errors to the various parameters derived to take this into account. Having pointed out that the distribution of probabilities has a rather broad maximum, it should also be emphasized, however, that the derived values of the parameters pass various consistency checks. For example, the most probable values for V_{sys} in the various directions derived here agree well with the values obtained in Sections 4.2 and 4.3.

(b) The most probable values for the non-circular systematic velocities derived above were the input for the next stage of simulations in which the dispersions ***(a)*** in the peculiar velocities, as well as R_l and R_h were varied. This was done mainly to verify the robustness of the conclusions of the previous set of simulations (Step IIIa). It turned out that the best fit values for the velocity dispersions agreed reasonably well with the values derived earlier from the analysis of the clouds in the null directions and the reflection nebulae. In Figures 4.12a to 4.12e we have shown the comparison between the cumulative distributions of the simulated population and that of the observed population for each of the ten sectors. To illustrate how sensitive the cumulative distributions are to the choice of the parameters, we have shown two fits for each direction: one a relatively good fit and the other somewhat poorer. The corresponding K-S probabilities are displayed on the top of each panel. The values of the parameters appropriate to each of the figures (figure 4.12a 4.12e) are summarised in Table 4.4.a and 4.4.b.

Table **4.4.a** : Parameters for the good fits.

Long. bins	1	2	3	4	5	6	7	8	9	10
V_{sys} (kms^{-1}) (fixed)	4.5	4.0	4.0	-3.5	-4.0	4.0	2.5	4.5	1.0	10.0
Probability(%)	100	100	98	100	91	92	100	100	100	100
a (kms^{-1})	2.5	3.0	4.0	6.0	5.5	5.0	4.5	4.5	4.5	8.0
R_L (pc)	150	250	200	100	250	250	250	300	1300	110
R_H (pc)	400	500	350	450	550	550	550	650	1600	360

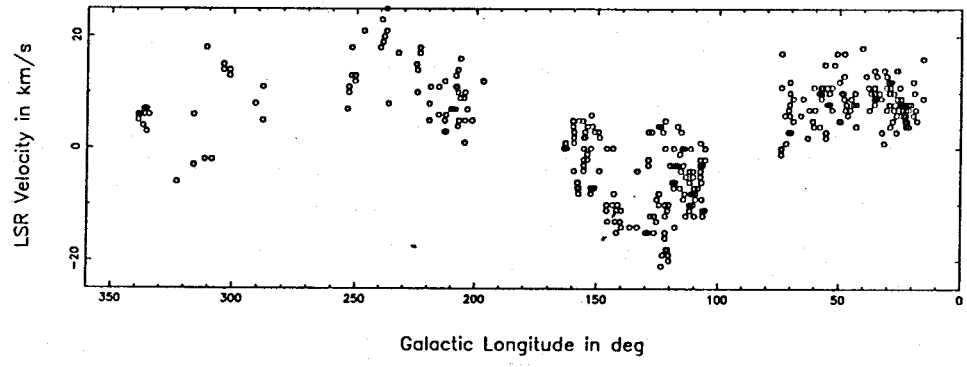

Fig.4.22.a : The longitude velocity plot of the observed population. The clouds in the *null directions* have not been shown.

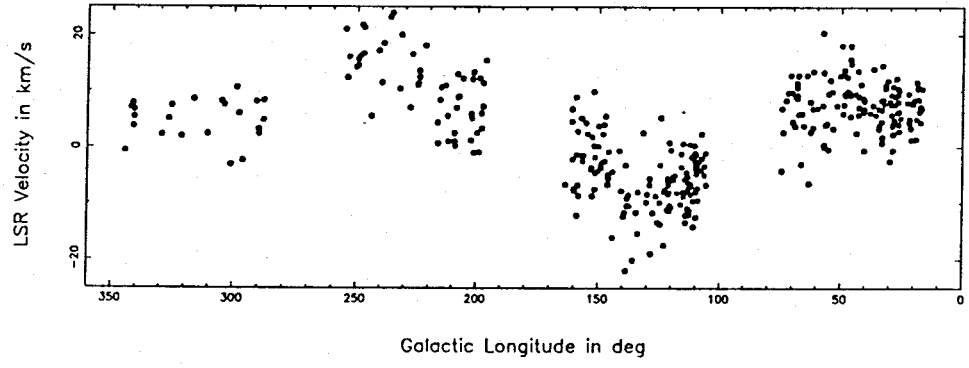

Fig.4.22.b : A *simulated* longitude-velocity plot. In each longitude sector, a population of clouds was generated using Monte Carlo methods: inner and outer boundaries of their distribution, the expansion velocity and the velocity dispersion were taken from Table 4.5.

Table **4.4.b** : Parameters for the poorer fits.

Long. bins	1	2	3	4	5	6	7	8	9	10
V_{sys} (kms^{-1}) (fixed)	4.5	4.0	4.0	−3.5	−4.0	4.0	2.5	4.5	1.0	10.0
Probability (%)	64	70	72	76	70	77	72	85	70	70
σ (kms^{-1})	4.0	4.5	6.0	8.0	7.5	7.0	6.5	6.5	6.5	8.0
R_L (pc)	200	250	100	150	200	350	300	150	1300	110
R_H (pc)	400	450	300	450	500	600	550	450	1500	260

A set of ten Tables given in Appendix D at the end of this thesis summarise the results of the simulations with the corresponding K-S probabilities for each of the ten directions. The final values of the parameters arrived at from these simulations are given in Table 4.5. Figure 4.13.a shows the plot of longitude distribution of velocities of the observed population of clouds while Fig.4.13.b shows the corresponding plot for a set of simulated population of clouds generated using the parameters given in Table 4.5.

Table **4.5** : Final fit parameters.

Longitudebins	1	2	3	4	5	6	7	8	9	10
V_{sys}(kms^{-1})	4.5	4.0	4.0	−3.5	−4.0	4.0	2.5	4.5	1.0	10.0
σ(kms^{-1})	2.5	3.0	4.0	6.0	5.5	5.0	4.5	4.5	4.5	8.0
$R_L(pc)$	150	200	130	150	250	250	250	300	1300	150
$R_H(pc)$	400	500	400	450	550	600	550	650	1600	400

Before summarizing the main conclusions of this Section let us recall our primary objective. In the previous Sections of this chapter, from an analysis of a subset of clouds in the four null directions, clouds with associated reflection nebulae, and some specific clouds from the composite CO survey, we had concluded that at least the clouds in these subsets were in a state of expansion with a velocity in the range 3 to 5 kms^{-1}, and that the velocity dispersion of these clouds is $\sim$ 2.5 to 5 kms^{-1}. In this Section we set out to establish whether these conclusions were more generally valid for the entire population of the local clouds. In addition, we also wished to derive a possible model for the spatial distribution of these clouds. The main conclusions of the detailed analysis presented in this section can be summarised as follows:

1. The population of the local dark clouds appear to be in a state of expansion about a common centre. Their radial velocity of expansion with respect to us is about 4 kms^{-1}.

2. In addition to their systematic motions (i.e. galactic rotation with a superimposed expansion velocity about a common centre) the clouds have peculiar or random velocities with a dispersion $\sim$ 2.5 to 5 kms^{-1}.

3. As to their spatial distribution, a model in which they are distributed in an oval-shaped doughnut with the Sun offset from the centre fits the data reasonably well. The distance to the inner edge of the doughnut varies from 150 to 300 pc, while to the outer edge varies from 400 to 600 pc depending upon the longitude.

4. In the longitude range 235° to 255°, most of the clouds in our sample appear to be unrelated to this system of expanding clouds, and are at a much greater distance of ~ 1.4 kpc.

5. A very intriguing feature of the local population of the dark clouds is that most of the clouds in the longitude range 100° to 145°, and some of the clouds in the range 195° to 215°, have negative radial velocities implying that they are approaching us.

References

Blanco,V.M. 1956, *Astrophys.J.*, **123**,64.

Dame, T.M., Ungrechts, H., Cohen, R.S., de Geus, E.J., Grenier, I.A., May, J., Murphy, D.C., Nyman, L.A., Thaddeus, P. 1987, *Astrophys.J.*, 322, 706.

de Vries,C.P., Brand,J., Israel, F.P., de Graauw,Th., Wouterloot,J.G.A., van de Stadt,H., Habing,H.J. 1984, *Astr. Astrophys.* Suppl., 56, 333.

Feitzinger, J.V. and Stuwe, J.A. 1986, *Astrophys.J.*, 305, 534.

Kutner,M.L., Machnik,D.E., Tucker,K.D., Dickman,R.L. 1980, *Astrophys.J.*, **237**, 734.

Petrie,R.M. 1965, Dominion *Astrophys.Obs.Publ.*, 12, 317.

Racine, R. 1968, *Astron.J.*, 73, 223.

Sahu, M.S. 1992, Ph.D. Thesis, University of Groningen.

Schmidt-Kaler,T. 1965, in Astronomie und Astrophysik, ed. H.H.Voigt, (Springer-Verlag, Berlin), p284.

Stark, A.A. 1984, *Astrophys.J.*, 281, 624.

Taylor, D.K., Dickrnan, R.L., Scoville, N.Z. 1987, *Astrophys.J.*, 315, 104.

van den Bergh, S., Herbst, W. 1975, *Astron.J.*, 80, 208.